Humidification-Dehumidification Desalination

John H. Lienhard V
Rohsenow Kendall Heat Transfer Laboratory,
Massachusetts Institute of Technology, Cambridge, MA 02139-4307 USA

Abstract

Humidification-dehumidification (HDH) desalination involves vaporizing water from a saline liquid stream into a carrier gas stream and then condensing the vapor to form purified water. This chapter describes various forms of the HDH cycle, with analysis of the energy consumption of various realizations of the process. The use of mass extraction/injection to improve performance is discussed. Analyses using both fixed component effectiveness and fixed component size are considered. Bubble column dehumidifiers are described, and the effect of very high feed salinity on energy and efficiency is discussed.

Keywords: Humidification-dehumidification desalination, Carrier gas extraction, Bubble column dehumidifier, Thermodynamic balancing, Mass injection and extraction, Effectiveness, Gained-output-ratio, Enthalpy pinch, Modified heat capacity rate ratio, High salinity

9.1 Introduction

Nature uses air as a carrier gas to desalinate seawater by means of the rain cycle. In the rain cycle, seawater gets heated (by solar irradiation) and evaporates into the air above to humidify it. Then the humidified air rises and forms clouds. Eventually, the clouds 'dehumidify' as rain, and that which falls over land can be collected for human consumption. The engineered version of this cycle is called the humidification-dehumidification desalination (HDH) cycle.

Humidification-dehumidification desalination technology has received wide attention in recent years. Although it does not compete with existing technologies, such as reverse osmosis, for desalinating brackish water or seawater in medium and large scale applications, HDH can be advantageous in decentralized, off-grid desalination applications where water treatment demand ranges up to several thousand cubic meters per day [1]. In addition, the technology does not use membranes and does not rely heavily on metal components, which allows it to treat highly saline water with some oil content without requiring expensive corrosion resistant materials. HDH has recently been commercialized and has succeeded in treating produced water from hydraulically fractured oil and gas wells [2].

A typical HDH system consists of a humidifier, a dehumidifier, and a heater. The simplest form of the HDH cycle is illustrated in Figure 9.1. The cycle consists of three subsystems: (a)

J.H. Lienhard, V, "Humidification-Dehumidification Desalination," in *Desalination: Water from Water*, 2nd edition, Chpt. 9, J. Kucera, editor. Hoboken, NJ: Wiley-Scrivener, 2019. ISBN 978-1-119-40774-4.

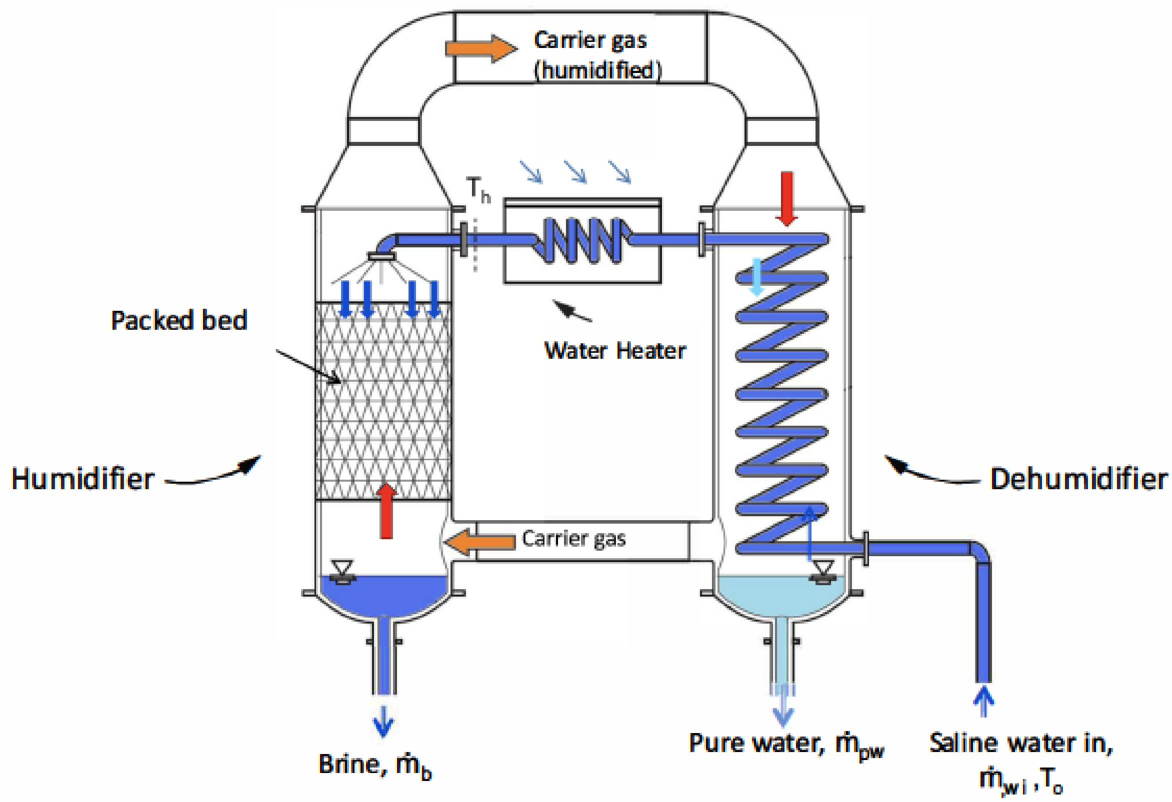

Figure 9.1: Simplest embodiment of HDH process [3].

the humidifier or evaporator; (b) the dehumidifier or condenser; and (c) an air and/or a brine heater (only a brine heater is shown in the figure), which can use various sources of energy such as solar power, natural gas, or geothermal heat, as well as combinations of these.

As shown in Fig. 9.1, cold air enters the humidifier where it is exposed to hot saline water, which increases the temperature and water content of the air. The hot moist air then enters the dehumidifier where it loses heat to a feed stream of cold saline water flowing through a coil. Water vapor condenses in the dehumidifier and exits the system as a stream of fresh liquid water. The more we preheat the saline water in the dehumidifier, the less heat we have to supply in the heater. Improving the energy efficiency of an HDH system is therefore, in part, a question of recovering and reusing the heat of condensation to heat the feed stream to the highest possible temperature before sending it to the heater.

Other configurations of HDH use a separate heat exchanger to preheat the feed using the warm condensate; this can enable a direct contact process in which cool fresh water is sprayed into the warm moist air allowing condensation on the droplet surface. Alternatively, the warm air can be bubbled up through cool fresh water to the same effect. Direct contact processes enable high rates of heat and mass transfer through minimal temperature differences. This highlights the second essential principle for keeping high energy efficiency in HDH: minimization of temperature and concentration differences associated with heat and mass transfer processes.

In recent years, many researchers have investigated HDH technology, as reviewed in [1,4]. However, the predecessor of HDH, the simple solar still, is also an engineered version of the rain cycle and has been studied far longer. The history of the transition from solar stills to HDH is summarized by Seifert et al. [5]. To understand the design objectives of the HDH system, some discussion of the shortcomings of the solar still is helpful.

Several papers have reviewed the numerous works on the solar still [6–8]. A solar still typically consists of an inclined glass cover above a pool of saline water. Sunlight passing through the glass heats the water, causing evaporation. The glass, being exposed to outside air, is cooler, and vapor condenses on its underside. The pure liquid is collected at the lower edge of the inclined glass.

The most prohibitive drawback of a solar still is its low thermal efficiency (Gained-output-ratio, or GOR[1], is often less than 0.5), which leads to a large surface area requirement. The low efficiency primarily the results of the loss of the latent heat of condensation to the environment through the glass cover of the still, so that absorbed energy is used just once. Some modified designs can recover and reuse the heat of condensation. These designs (called multi-effect stills) achieve some increase in the thermal efficiency, but the overall energy efficiency is still relatively low.

The solar still's poor efficiency is accentuated because the various functional processes—solar absorption, evaporation, condensation, and heat recovery—all occur within a single component. Moist air flow is uncontrolled, and sensible heat is readily lost from the warm saline water to the glass and from there to the environment. By separating these functions into distinct components, thermal inefficiencies may be reduced and overall performance improved. This separation of functions is the essential characteristic of the HDH system. For example, the recovery of the latent heat of condensation, in the HDH process, is effected in a separate heat exchanger (e.g., the dehumidifier) wherein the saline feedwater can be preheated. The module for heat input (a solar collector or other heat exchanger) can be optimized almost independently of the humidification and dehumidification components. Both the dehumidifier and humidifier can be optimized as individual components. The HDH process, thus, promises higher energy efficiency as a result of the separation of the basic processes.

HDH systems have sometimes been categorized as small scale systems (< 1 m^3/day), but both the initial and current history contradict this. During the early 1960's, an 18 m^3/day solar-heated HDH pilot was built in Puerto Peñasco, Mexico by Hodges and coworkers from the University of Arizona [9]. More recently, Gradiant Corporation has used HDH systems larger than 2,000 m^3/day to purify produced water from oil and gas operations, at salinities from 100,000 to 250,000 mg/kg [2,10]. Further, recent designs are generally modular and can be scaled-up without limitation by adding additional modules.

9.1.1 Classification of HDH cycles.

HDH processes are often classified by the cycle configuration selected (Figure 9.2). As the name suggests, an open-air (OA) cycle is one in which ambient air is taken into the humidifier, where it is heated and humidified, and then sent to the dehumidifier, where it is partially

[1]See Sec. 9.1.2 for the definition of GOR.

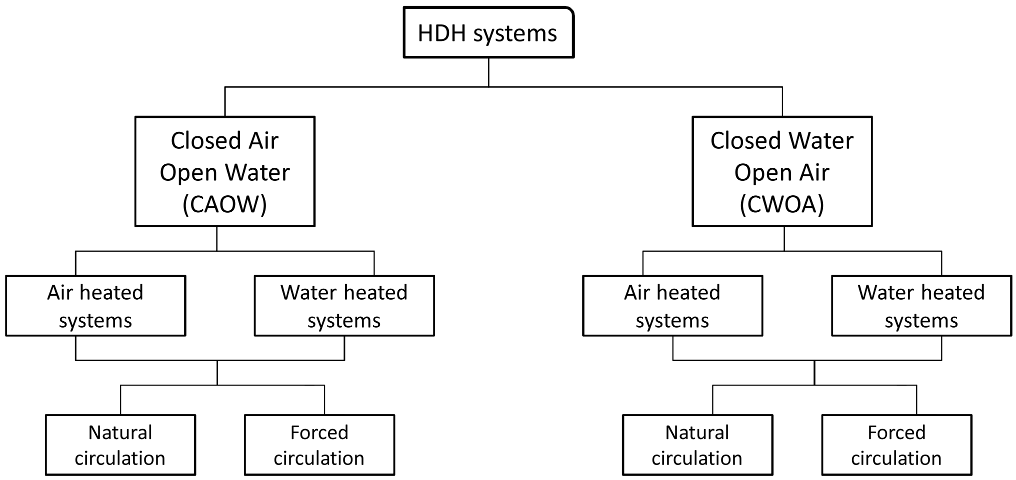

Figure 9.2: Classification of HDH systems based on cycle configurations [1].

dehumidified and let out. A closed air (CA) cycle is a cycle wherein the air is circulated in a closed loop between the humidifier and the dehumidifier. In a closed water (CW) cycle, the brine is recirculated until a desirable recovery is attained, using make-up water in proportion to the pure water recovered. Because the single-pass water recovery of HDH is low (on the order of 5%), brine recycling is necessary for applications that require significant water recovery ratios. Such cycles may involve heat rejection or recovery after the brine leaves the humidifier outlet. In particular, if the brine is returned to a fixed temperature prior to the inlet of the dehumidifier, the closed-water cycle performs much like an open-water cycle drawing intake water at that fixed temperature.

The air in these systems can be circulated by either natural convection or mechanical blowers, and feedwater is typically circulated by a pump. Although forced air flow increases the demand for electrical power, a stable air flow may be advantageous because the energy efficiency of HDH is extremely sensitive to the water-to-air mass flow rate ratio. Understanding the relative technical advantages of each of these cycles is pivotal to choosing the configuration that is best in terms of energy efficiency and cost of water production under given operating conditions.

The third classification of the HDH systems is based on the type of heating used: water or air heating systems. The performance of the system depends greatly on the placement of the heater within the respective flow loops.

9.1.2 System-Level Performance Parameters

The following performance parameters are used to characterize HDH systems.

1. Gained-Output-Ratio (GOR): is the ratio of the latent heat of evaporation of the water produced to the net heat input to the cycle.

$$\mathrm{GOR} \equiv \frac{\dot{m}_{pw} \cdot h_{fg}}{\dot{Q}_{in}} \tag{9.1}$$

This parameter is, essentially, the thermal energy effectiveness of water production. Higher values are better, indicating a greater degree of heat recovery in the system. This is the primary performance parameter of interest in HDH (and to thermal desalination systems, in general). GOR is very similar to the performance ratio (PR) defined for MED and MSF systems. For steam-driven desalination systems (like in most state-of-the-art MSF and MED systems), PR is approximately equal to GOR:

$$\mathrm{GOR} = \frac{\dot{m}_{pw} \cdot h_{fg}}{\dot{m}_s \cdot \Delta h_s} \tag{9.2}$$

$$\approx \frac{\dot{m}_{pw}}{\dot{m}_s} \tag{9.3}$$

It is worthwhile to note that GOR is equivalent to the ratio of the latent heat (h_{fg}) to the specific thermal energy consumption (thermal energy input per unit water produced). The latent heat in the equations above is calculated at the average partial pressure of water vapor (in the moist air mixture) in the dehumidifier.

2. Recovery ratio (RR): is the ratio of the amount of water produced per kg of feed. This parameter is also called the extraction efficiency [11]. The RR is, generally, found to be around 5% for the HDH system in single pass and can be increased to higher values (up to 90% depending on feed salinity) by brine recirculation.

$$\mathrm{RR} \equiv \frac{\dot{m}_{pw}}{\dot{m}_w} \tag{9.4}$$

3. Specific electricity consumption, SEC: is the amount of electrical power required to run blowers and pumps per unit mass of pure water produced. Denoting this power as $\dot{W}_e$:

$$\mathrm{SEC} = \frac{\dot{W}_e}{\dot{m}_{pw}} \tag{9.5}$$

The electrical energy use is thermodynamically distinct from the thermal energy use (and has a different price). The two should not be directly added when considering the energy efficiency of a thermal desalination system (see [12] for details). Data for SEC in open literature are limited.

Based on a previous literature review [1], we can benchmark the key performance metrics of existing HDH systems: (1) the cost of water production; (2) the heat and mass transfer rates in the dehumidifier; and (3) the system energy efficiency (GOR).

The total cost of water production in HDH systems is principally a sum of the energy cost (captured by the GOR of the system) and the capital cost.[2] A large fraction of the capital

[2]The HDH system has relatively minimal maintenance requirements.

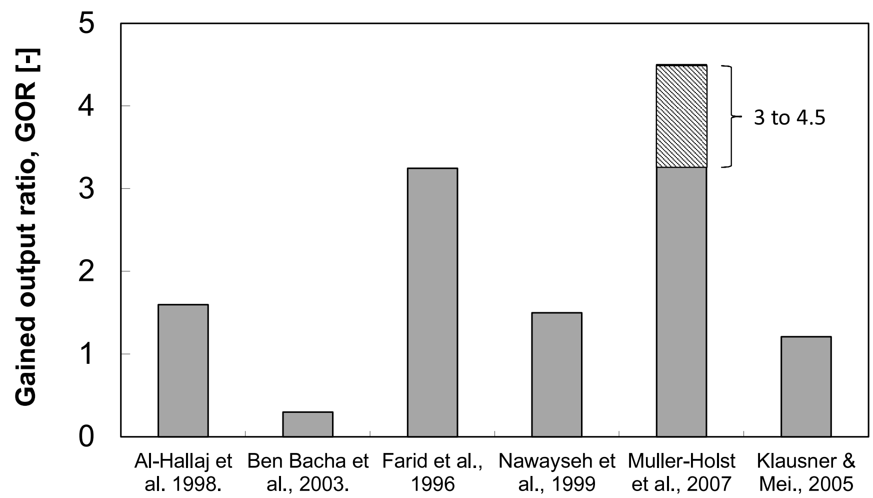

Figure 9.3: Performance of the older HDH systems in the literature [3].

investment in typical HDH systems is the dehumidifier cost. This cost is driven by the low heat and mass transfer rates common in such devices. The 'equivalent' heat transfer coefficient in the dehumidifier has been reported to lie between 1 and 100 W/m^2K [13, 14]. This is two orders of magnitude lower than for pure vapor condensers.

Using the data given in various papers, GOR for the reported systems was calculated. The maximum GOR among existing HDH systems was about 3. Figure 9.3 illustrates the GOR of a few of the studies. The GOR varied between 1.2 to 3. These values of GOR translate into energy consumption rates from 215 kWh_{th}/m^3 to 550 kWh_{th}/m^3. The low value of GOR achieved by Ben Bacha et al. [15] was because they did not recover the latent heat of condensation. Instead, they used separate cooling water from a well to dehumidify the air. Lack of a systematic understanding of the thermal design of HDH systems, which can help to optimize performance, is the reason behind such inefficient designs. The higher value of GOR achieved by Müller-Hölst et al. [16] was because of higher heat recovery and efforts to reduce the temperature differences between the air and water streams. These results tell us the importance of maximizing heat recovery in minimizing the energy consumption and the operating and capital cost of HDH systems. It is also to be noted that the GOR fluctuated between 3 to 4.5 in Müller-Hölst's system because of the inability of that system to independently control the air flow under the natural convection design that was applied. It is, therefore, desirable to develop forced convection based systems which have a sustainable peak performance.

Based on a simple thermodynamic calculation, the GOR of a thermodynamically reversible HDH system can be evaluated to be 122.5 for typical boundary conditions [17]. When compared to a GOR of 3 for existing systems, the reversible GOR of 122.5 shows that there is significant potential for improvement to existing HDH systems in terms of reducing thermodynamic losses. This observation gives ample motivation to study the thermal design of these systems in detail.

A few studies in literature actually report the overall cost of water production in a HDH system [16, 18, 19]. This cost is found to be about $30 per cubic meter of water produced, which is very high. More recent work, based on systems with higher energy efficiency, suggests that the costs can be reduced below $5 per cubic meter [20]. HDH is often used for high salinity wastewater from oil and gas operations, a setting in which treated water carries a high premium. Together with the robustness and low capital cost of the system, HDH is attractive in that setting.

9.1.3 Improving the energy efficiency of HDH systems

As suggested above, the irreversibility—the entropy generation rate—of HDH systems decreases the GOR below its thermodynamically reversible level. Mistry et al. [21, 22, 23] found that the highest energy efficiency was achieved when the entropy generation per unit mass of product was minimized and that most of the entropy generated in an HDH system was a result of the heat and mass transfer in the dehumidifier and the humidifier. Entropy generation in these components occurs because heat and mass are transferred through finite differences in temperature and concentration. Thiel and Lienhard [24] showed that a larger portion of the entropy generation in the dehumidifier is a result of the mass transfer by diffusion due to the presence of high concentrations of air. This led to the conclusion that it is more important to balance the humidity ratio difference than the temperature difference. Narayan et al. [25] defined a modified control-volume based heat capacity rate ratio, HCR, and found that the entropy generation per unit water produced in a heat and mass exchanger with fixed inlet conditions and energy effectiveness was minimized at HCR = 1. The HCR is discussed in Section 9.2.

Further, because the water content of saturated air is a nonlinear function of temperature, temperature and concentration differences vary along the length of the component. A number of studies have looked at varying the water-to-air mass flow rate, m_r, ratio within the component to decrease these differences and thus lower entropy generation. The Puerto Peñasco HDH system previously mentioned included four extractions of air from the humidifier to the dehumidifier [8, 9]. Müller-Holst [16, 26] cited the variability of the stream-to-stream temperature difference as a major source of entropy generation and suggested the continuous variation of the mass flow rate of air through extraction/injection to keep the stream-to-stream temperature difference constant throughout the system. Zamen et al. [27] modeled a multi-stage system with each stage operating at a different water-to-air mass flow rate ratio. The model fixed a temperature pinch[3] and used up to four stages.

McGovern et al. [28] used temperature-enthalpy diagrams to represent the process paths of the water and air streams. They studied the variation of the performance of the system with the pinch point temperature difference and with the implementation of a single water extraction. Narayan et al. [29] expanded on that finding by defining an enthalpy pinch and suggesting that it was the correct pinch to balance at the two ends of a heat and mass exchanger as it takes into account the transfer of both heat and mass. Working from this model, Narayan et al. [30] experimentally increased the energy efficiency of a system of fixed size by 54% by using a single air extraction. Similarly, Chehayeb et al. [31] used a fixed enthalpy pinch model to study the performance of systems with up to 5 extractions/ injections. The enthalpy pinch model is discussed in Section 9.3.

[3]The pinch point is the minimum temperature difference between the air and water streams within a component. For the dehumidifier the pinch point will always be at either the inlet or the outlet of the device. For the humidifier, the pinch point will generally be internal to the device (see Figure 9.18).

9.1.4 Components of the HDH system

Any HDH cycle will include a humidifier and a dehumidifier. The humidifier commonly consists of a packed bed. Water is sprayed into the top of the packing, with air entering in counterflow at the bottom of the packing. Modeling of this component can be done by standard means, for example, by using the Poppe-Rögener model with the Kloppers-Kröger algorithm as developed for cooling towers [32–36]. The packing can be of a variety types, but is generally an inexpensive polymeric material having sufficient open area to minimize air pressure drop while providing a large, compact surface area from which evaporation occurs. A major advantage of the packed bed humidifier is that scaling or fouling on the surface of the packing material does not impede heat and mass transfer from the air-water interface. Further, because the packed bed operates at atmospheric pressure and modest temperature, low cost structural material can be employed. Expensive, corrosion-resistant metals are not required.

The dehumidifier is a more problematic component that requires a higher level of thermal design. The key challenge of a dehumidifier is the presence of incondensable gas (air), which tends to accumulate at the condenser surface as water vapor is taken out as liquid water. Concentration of air near the condenser surface greatly impedes heat and mass transfer. To compensate for this effect, a typical HVAC dehumidifier uses large areas of metal condenser plates (or fins) to lower the gas side transport resistance. The plates add both bulk and cost to the system. An alternative approach is to employ a direct contact condensation process. Klausner et al. [11, 37] used counterflow of pure water and moist air through a packed bed. Water vapor condensed directly on the falling liquid film, giving less opportunity for incondensable gas accumulation while yielding high heat and mass transfer coefficients. A more recent approach has been to use bubble columns, in which moist air is sparged into cool fresh water, leading to condensation on the bubbles' surfaces. By using a series of three to five spargers in a counterflow arrangement, very efficient condensation and excellent recovery of latent heat of condensation are achieved. The water layers are kept shallow to limit air-side pressure drop. The basic design is similar to that of a low-profile air stripper. Bubble columns are compact and inexpensive, and a result this technology has found industrial-scale application for HDH. Bubble columns are discussed in Section 9.4.

9.2 Thermal Design

When finite time thermodynamics is used to optimize the energy efficiency of thermal systems, the optimal design is one which produces the minimum entropy within the constraints of the problem (such as fixed size or cost). In this section, we apply this well-established principle to the thermal design of combined heat and mass exchange devices (dehumidifiers, and humidifiers) for improving the energy efficiency of HDH desalination systems. The theoretical framework for design of heat and mass exchange (HME) devices for implementation in the HDH system has been developed in a series of recent papers [17, 21, 22, 24, 25, 28–31, 35, 36, 38]. The linchpin in this theoretical work is the definition of a novel parameter known as the 'modified heat capacity rate ratio' (HCR). A brief summary of the definition of this parameter and its significance to thermal design of HME devices and the HDH system is given below.

Modified heat capacity rate ratio In the limit of infinite heat transfer area, the entropy generation rate in a regular heat exchanger will be entirely due to what is known as thermal imbalance. Imbalance is associated with conditions for which the heat capacity rates of the streams exchanging heat are not equal [39]. In other words, a heat exchanger (with constant specific heat capacity for the fluid streams) is said to be thermally 'balanced' at a heat capacity rate ratio of one. This concept of thermodynamic balancing, very well known for heat exchangers, was extended to HME devices by Narayan et al. [17].

In order to define a thermally 'balanced' state in HME devices, a modified heat capacity rate ratio (HCR) for combined heat and mass exchangers was defined by analogy to heat exchangers as the ratio of the maximum change in the total enthalpy rate of the cold stream to that of the hot stream.

$$\mathrm{HCR} = \frac{\Delta \dot{H}_{\mathrm{max},c}}{\Delta \dot{H}_{\mathrm{max},h}} \tag{9.6}$$

The maximum changes are defined by identifying the ideal states that either stream can reach at the outlet of the device. For example, the ideal state that a cold stream can reach at the outlet will be to match the inlet temperature of the hot stream and that a hot stream can reach at the outlet will be to match the inlet temperature of the cold stream. The physics behind this definition is explained in detail in [17].

The value of HCR will change when the water-to-air mass flow rate ratio, m_r, changes. For this reason, many investigators have reported changes in the energy efficiency of HDH cycles with m_r. These changes can only be understood systematically by considering HCR instead of m_r, as shown in later sections.

HME devices can be studied under the constraint of a fixed performance (with size varying to maintain this performance under varying inlet conditions) or as a fixed piece of hardware (with varying performance under varying inlet conditions). The former is known as an on-design analysis and the latter is known as an off-design analysis. Section 9.2.1 reviews an on-design model developed by Narayan and coworkers [17, 29, 38], the energy effectiveness model. Section 9.2.2 reviews an off-design model from Chehayeb and coworkers [35, 36]. For details of the analysis, the reader is referred to the relevant papers.

9.2.1 Effectiveness Model (On-Design Model)

An energy-based effectiveness, analogous to the effectiveness defined for heat exchangers, is given as:

$$\varepsilon = \frac{\Delta \dot{H}}{\Delta \dot{H}_{\mathrm{max}}} \tag{9.7}$$

This definition is based on the maximum change in total enthalpy rate that can be achieved in an adiabatic heat and mass exchanger. Effectiveness is the ratio of change in total enthalpy rate ($\Delta \dot{H}$) to the maximum possible change in total enthalpy rate ($\Delta \dot{H}_{\mathrm{max}}$). The maximum possible change in total enthalpy rate will refer to the cold or the hot stream, depending on the heat capacity rate of the two streams. The stream with the minimum heat capacity rate dictates the thermodynamic maximum amount of heat transfer that can be attained between the fluid streams. This concept was introduced in [38] and subsequently generalized by Chehayeb et al. [36] to account for internal pinch points (as can occur in a humidifier; see Fig. 9.18). For a situation with terminal pinch points, $\Delta\dot{H}_{\text{max}}$ will simply be the smaller of $\Delta\dot{H}_{\text{max,c}}$ and $\Delta\dot{H}_{\text{max,h}}$. More generally,

$$\Delta\dot{H}_{\text{max}} = \Delta\dot{H}_{\text{pinch}} \tag{9.8}$$

This latter formulation is always preferred.[4]

The thermodynamic performance of some representative HDH cycles are now analyzed by way of a theoretical cycle analysis. Control-volume based models for the humidifier and the dehumidifier are used to perform this analysis. The governing equations for the control-volume based models are presented in detail in previous publications [17, 38].

In performing the analysis, the following approximations have been made:

- The processes operate at steady-state conditions.
- There is no heat loss from the humidifier, the dehumidifier, or the heater to the ambient.
- Pumping and blower power are not considered.
- Kinetic and potential energy terms are neglected in the energy balance.
- The water condensed in the dehumidifier is assumed to leave at a temperature which is the average of the humid air temperatures at inlet and outlet of the dehumidifier.
- It was previously shown that the use of pure water properties instead of seawater properties does not significantly affect the performance of the HDH cycle at optimized mass flow rate ratios [21]. Hence, only pure water properties are used in the on-design calculations. The effect of salinity becomes important through boiling point elevation for more saline feedwaters [40].

9.2.1.1 Water Heated HDH Cycle

One of the most commonly studied HDH cycles is the closed-air open-water water-heated (CAOW) cycle (see Figure 9.4). A comprehensive study of parameters which affect the performance of this cycle will help to understand the ways by which the performance of this basic cycle can be improved. The parameters studied include top and bottom temperatures of the cycle, mass flow rate of the air and water streams, the humidifier and dehumidifier effectivenesses and the operating pressure. The performance of the cycles depends on the mass flow rate ratio (ratio of mass flow rate of seawater at the inlet of the humidifier to the mass flow rate of dry air through the humidifier), rather than on individual mass flow rates. Hence, the mass flow rate ratio is treated as a single variable. This variation with mass flow rate ratio has been noted by many investigators [21, 41–43].

Effect of relative humidity of the air entering and exiting the humidifier ($\varphi_{a,1}, \varphi_{a,2}$) The humidifier and dehumidifier can readily be designed such that the relative humidity of air at their exit is one. Hence, the exit air from these components is usually considered to be saturated when analyzing these cycles. However, the exit relative humidity is indicative of

[4]Failure to account for internal pinch points can lead to unphysical results, such as negative entropy generation.

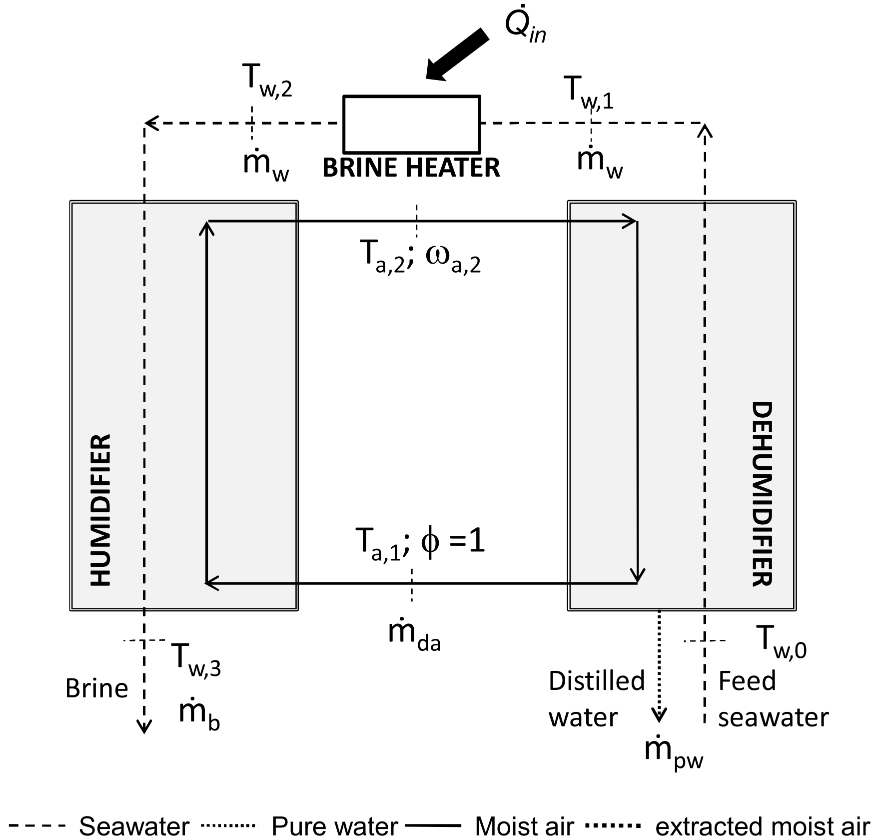

Figure 9.4: Schematic diagram of a water-heated closed-air open-water HDH cycle [17].

the performance of the humidifier and the dehumidifier; and hence, understanding how the variation of these parameters changes the performance of the system is important.

Figure 9.5 illustrates the effect that relative humidity of air at the humidifier inlet and exit can have on the performance of the cycle (GOR). For this particular case, the top ($T_{w,2}$) and bottom temperatures ($T_{w,0}$) were fixed at 80 °C and 35 °C respectively. Humidifier and dehumidifier effectivenesses ($\varepsilon_h, \varepsilon_d$) were fixed at 90%. Mass flow rate ratio was fixed at 5. It can be observed that for a variation of $\varphi_{a,2}$ from 100 to 70% the performance of the system (GOR) decreases by roughly 3%, and for the same change in $\varphi_{a,2}$ the effect is roughly 34%.

This difference suggests that the relative humidity of the air at the inlet of the humidifier has a much larger effect on performance. These trends were found to be consistent for all values of mass flow rate ratios, temperatures and component effectivenesses. This, in turn, suggests that the dehumidifier performance will have a larger impact on the cycle performance. This issue is further investigated in the following paragraphs.

Effect of component effectiveness ($\varepsilon_h, \varepsilon_d$) Figure 9.6 and 9.7 illustrate the variation of performance of the cycle at various values of component effectivenesses. In Figure 9.6, the top temperature is fixed at 80 °C, the bottom temperature is fixed at 30 °C and the dehumidifier

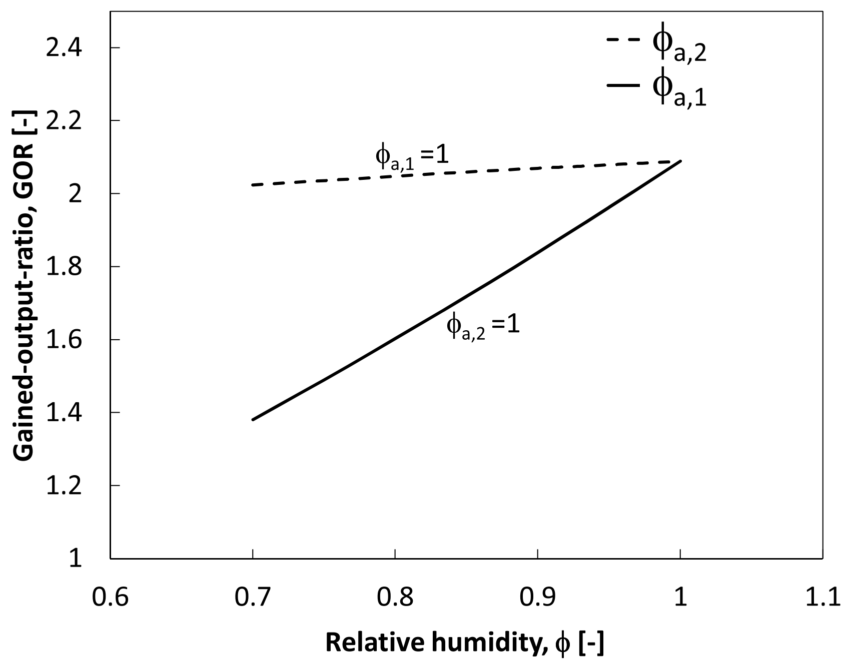

Figure 9.5: Effect of relative humidity on performance of the WH-CAOW HDH cycle.

effectiveness is fixed at 80%. The mass flow rate ratio was varied from 1 to 6. It is important to observe that there exists an optimal value of mass flow rate ratio at which the GOR peaks. It can also be observed that the increase in performance is fairly linear with increasing humidifier effectiveness, ε_h. In Figure 9.7, the top temperature is fixed at 80 °C, the bottom temperature is fixed at 30 °C and the humidifier effectiveness is fixed at 80%. The cycle performance changes more dramatically for higher values of dehumidifier effectiveness. These trends are consistent for various values of top and bottom temperatures. Hence, a higher dehumidifier effectiveness is more valuable than a higher humidifier effectiveness for the performance (GOR) of the cycle.

In the previous discussion, we have observed that the dehumidifier exit air relative humidity ($\varphi_{a,1}$) is more important than the humidifier exit air relative humidity ($\varphi_{a,2}$). Hence, based on these results, we can say that for a water heated cycle the performance of the dehumidifier is more important than the performance of the humidifier.

Effect of top temperature ($T_{w,2}$) Figure 9.8 illustrates the effect of the top temperature on the cycle performance (GOR). For this particular case, the bottom temperature ($T_{w,0}$) was fixed at 35 °C and humidifier and dehumidifier effectivenesses were fixed at 92%. Top temperature ($T_{w,2}$) was varied from 50 °C to 90 °C. The optimal value of mass flow rate ratio increases with an increase in top temperature. Depending on the humidifier and dehumidifier effectiveness itself this trend changes. At lower component effectivenesses, the top temperature has no or little effect on the cycle performance. This result is counter-intuitive. However, it can be explained

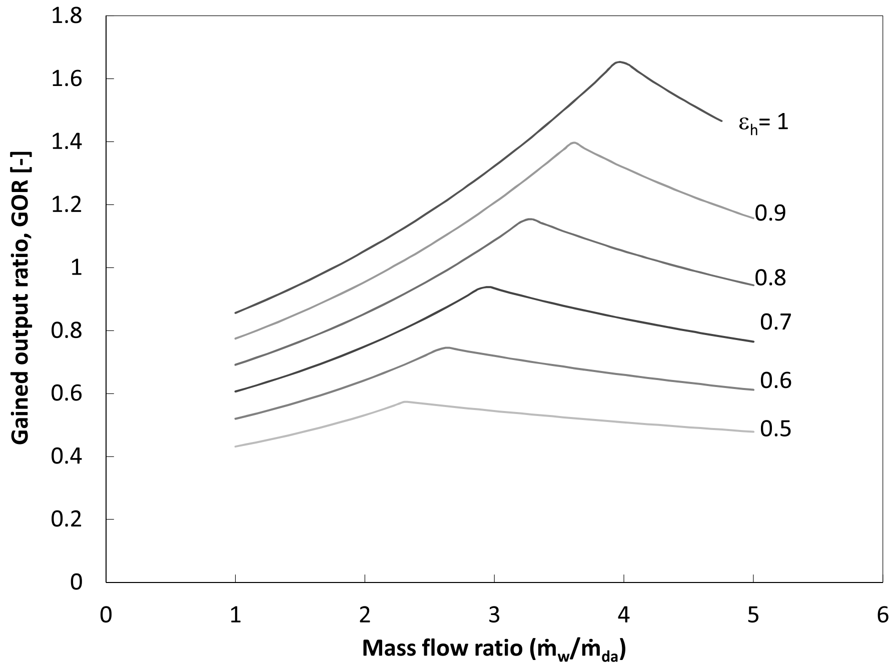

Figure 9.6: Effect of component effectiveness of humidifier on performance of the WH-CAOW HDH cycle [17].

using the modified heat capacity rate ratio.

The modified heat capacity rate ratio (HCR) is the ratio of maximum possible enthalpy change in the cold stream to the maximum possible enthalpy change in the hot stream. It was found that the entropy generation in a heat and mass exchange device is minimized (for a given effectiveness and inlet conditions) when HCR = 1 ('balanced' condition). We will use this understanding to explain the trends obtained at various top temperatures.

Figure 9.9 shows the variation of GOR with the heat capacity rate ratio of the dehumidifier (HCR_d). It can be seen that GOR reaches a maximum at $\mathrm{HCR}_d = 1$. The maximum occurs at a balanced condition for the dehumidifier which, as we have shown in the preceding paragraphs is the more important component. Chehayeb et al. [36] explain in detail the reasons for the dominance of HCR_d. The irreversibility of the humidifier (and the total irreversibility of the system) increases with an increase in top temperature. A system with higher total irreversibility has a lower GOR [21]. This explains the decrease in GOR with an increase in top temperature. The reader should take note that this trend occurs for fixed component effectiveness. For a fixed component size, GOR increases with top temperature (see discussion in Section 9.2.2.3).

Also, as the top temperature increases, the dehumidifier is balanced at higher mass flow ratio and hence the optimum value of GOR occurs at higher mass flow ratios.

Effect of bottom temperature ($T_{w,0}$) The bottom temperature of the cycle ($T_{w,0}$) is fixed by the feedwater temperature at the location where the water is drawn. Figure 9.10 illustrates a case with top temperature of 80 °C and component effectivenesses of 92%. A higher bottom

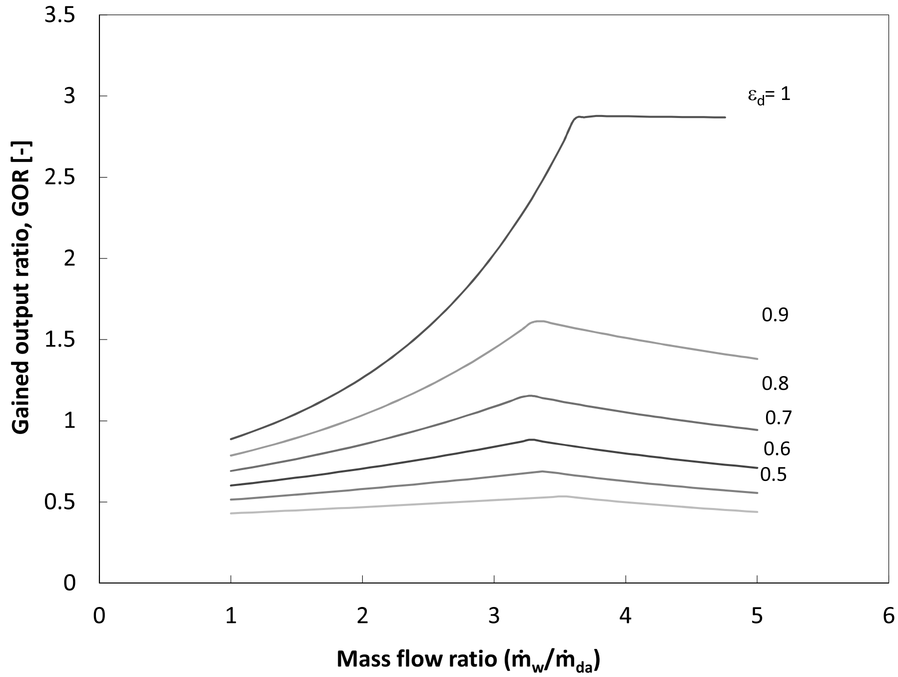

Figure 9.7: Effect of component effectiveness of dehumidifier on performance of the WH-CAOW HDH cycle [17].

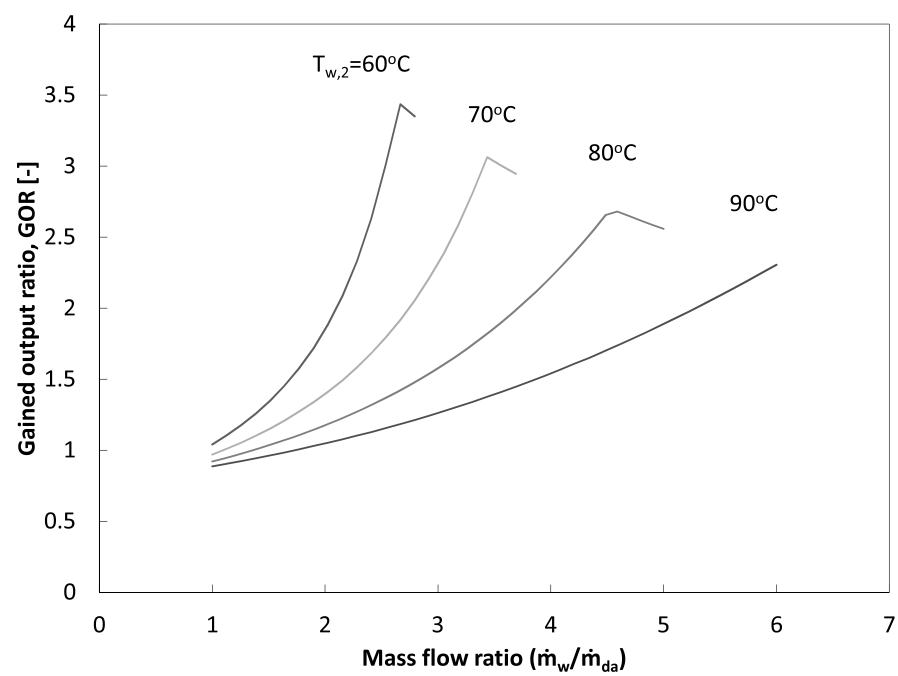

Figure 9.8: Effect of top brine temperature on performance of the WH-CAOW HDH cycle [17].

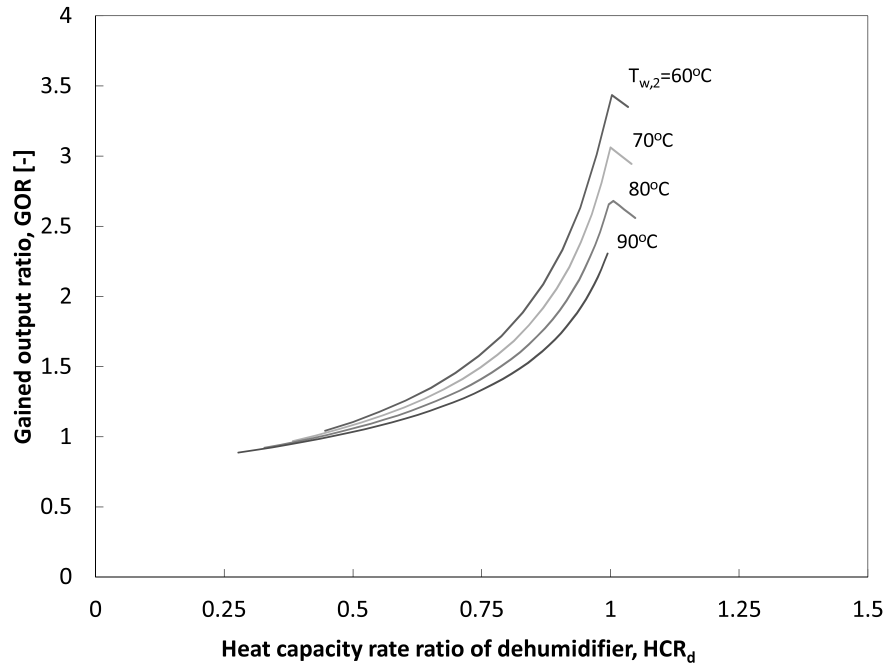

Figure 9.9: HCR of dehumidifier versus GOR at various top brine temperatures [17].

temperature of the cycle results in a higher value of GOR as illustrated in the figure. This result can again be understood by plotting HCR of the dehumidifier versus the GOR of the system (Figure 9.11). The degree of balancing of the humidifier at the optimum condition for GOR decreases with a decrease in bottom temperature. Hence, the irreversibilities in the humidifier (and the total irreversibility of the system) increase with decreasing bottom temperature, and the GOR declines.

From these studies, the performance of the cycle (GOR) has a functional dependence as follows:

$$\mathrm{GOR} = f(\mathrm{HCR}_h, \mathrm{HCR}_d, \varepsilon_h, \varepsilon_d, T_{w,2}, T_{w,0}, \varphi_{a,2}, \varphi_{a,1}) \tag{9.9}$$

The numerically computed values of GOR reported in this section for the CAOW water-heated cycle are within 20% of the experimental value obtained by Nawayseh et al. [44] for the same boundary conditions.

9.2.1.2 Single and multi-stage air-heated cycles

A simple air-heated cycle is one in which air is heated, humidified, and dehumidified [18, 19, 45, 46]. A number of earlier studies found that the GOR for some realizations of this cycle is very low (GOR<1; only slightly better than a solar still). The performance, however, is significantly affected by the location of the air heater, as discussed by Narayan et al. [17] and Mistry et al. [21]. Significantly better performance is obtained if the air is heated after the moist air leaves the humidifier and before it enters the dehumidifier. The reason is that if the air is heated upstream of the humidifier, evaporation in the humidifier tends to cool the air as it passes through: heat

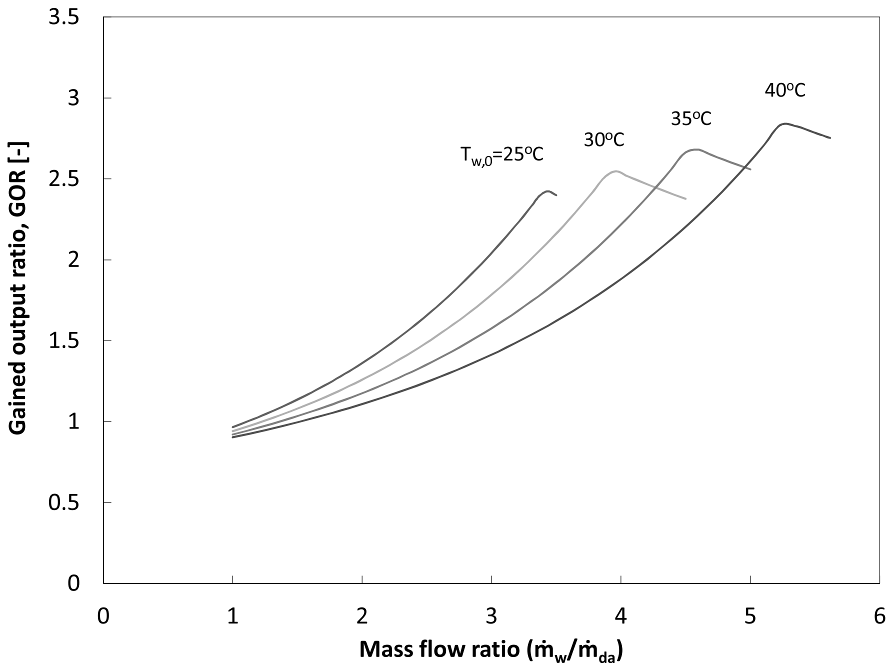

Figure 9.10: Effect of feedwater temperature on performance of the WH-CAOW HDH cycle [17].

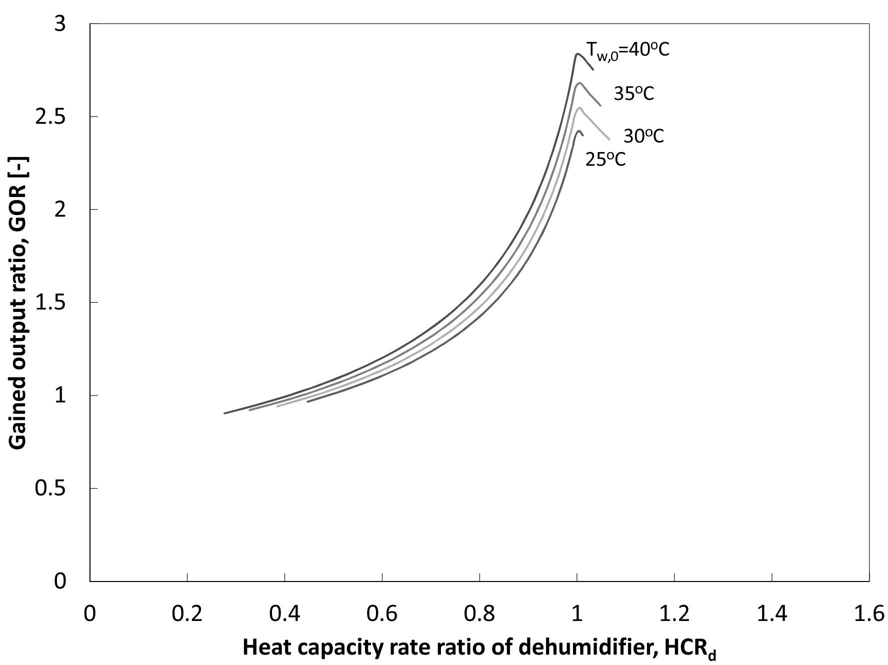

Figure 9.11: HCR of dehumidifier versus GOR at various feedwater temperatures [17].

Table 9.1: Optimization results for water-heated and air-heated CAOW cycles as a function of the minimum terminal temperature difference in either the humidifier or the dehumidifier [22].

	Minimum Terminal Temperature Difference					
	CAOW-WH			CAOW-AH		
Parameter	4 K	5 K	6 K	4 K	5 K	6 K
GOR	3.50	3.14	2.85	3.83	2.98	2.44
$\dot{S}_{gen}$ [kW/K]	0.25	0.30	0.35	0.28	0.35	0.41
m_r	3.67	4.42	5.29	1.46	1.24	1.07
ε_D	0.96	0.96	0.96	0.93	0.89	0.85
ε_H	0.90	0.89	0.88	0.91	0.88	0.85
T_{min} [K]	303.15	303.15	303.15	303.15	303.15	303.15
T_{max} [K]	345.28	350.77	355.65	370.15	370.15	370.15

is lost to the brine stream. In the other arrangement, heat is instead transferred to the saline water feed, assisting in heat recovery.

Mistry et al. [22] used nonlinear programming techniques to perform a full numerical optimization of several variations of HDH cycles that used air-heating, including the CAOW cycle in Fig. 9.4. Their simulations were based on a fixed terminal temperature difference (or TTD; this is another type of on-design model). Systematic use of optimization methods identified operating conditions more favorable than in previous studies. Their results for CAOW-air-heated and CAOW-water-heated cycles are compared in Table 9.1.

In general, all these results are obtained at high component effectiveness. Further, as might be expected, the best performance is obtained at low TTD. Both low TTD and high effectiveness tend to imply larger components. However, for the humidifier a greater concern relates to the processes within the control volume used by on-design models. Counterflow humidifiers of cooling tower style will have an internal pinch point (see Fig. 9.18) that precludes low values of TTD when the air temperature rise is large; a more representative TTD might be 10 K or more in those situations. Assigning a very small TTD to such a device implies that an internal temperature cross (or negative entropy generation) occurs, which is physically impossible. On the hand, the results in Table 9.1 satisfy the second law of thermodynamics on a control volume basis, leaving open the possibility that some [as yet unknown] heat and mass exchanger could be developed to operate between the given inlet and outlet states. We provide Table 9.1 simply to illustrate the role of TTD and its influence on GOR.

Chafik [18,47] proposed a multi-stage air-heated cycle. The air in this cycle is heated and sent to a humidifier where it becomes saturated. The air is then further heated and humidified again. The idea behind this scheme was to increase the exit humidity of the air so that water production can be increased. As discussed Nayaran et al. [17], Chafik was able to increase the exit humidity from 4.5% (by weight) for a single stage system to 9.3% for a 4 stage system, but the GOR of the cycle rose by only 9% because the increased water production comes at the cost of increased energy input. Multi-staging does not improve the heat recovery in the humidification process. Chafik reported a very high cost of water production (28.65 €/m^3) caused in part by the low energy efficiency of the system.

9.2.1.3 Varied pressure cycles and other carrier gases

On-design models have also been used to explore varied pressure operation of HDH [17, 48, 49, 50]. Both reduced pressure and varied pressure cycles have been shown to increase GOR. For the varied pressure cycle, the pressure is lowered in the humidifier, so that the water mass fraction will be greater for a given saturated air temperature, and pressure is raised in the dehumidifier, so as to encourage condensation. Simulation results from these studies were promising, showing very substantial increases in GOR when high efficiency compressors and expanders were used. Both mechanical compressors and thermocompressors [51, 52] were examined. However, the compression ratios needed for optimal performance were quite modest (on the order of 1.2 or so), and the available compressors and expanders lack sufficient efficiency to achieve the predicted gains in energy efficiency [53].

The potential use of carrier gases other than air has also been considered. Among these, helium shows significant advantages in its thermophysical properties [54]. Air, however, remains the most practical choice for a carrier gas.

9.2.1.4 Summary of on-design findings

The fixed effectiveness and the fixed TTD models lead to the following general conclusions. The performance of a basic water-heated cycle depends on: (a) the water-to-air mass flow rate ratio; (b) the humidifier and dehumidifier effectivenesses; (c) top and bottom temperatures; and (d) relative humidity of air at the exit of the humidifier and the dehumidifier. At a specific value of the water-to-air mass flow rate ratio, m_r, the energy efficiency of the system is maximized. This optimal point is characterized by a thermodynamically balanced condition in the dehumidifier. The balanced condition occurs at a modified heat capacity rate ratio of 1. This finding is extremely important, as it is also fundamental to design of both single-stage systems and in the algorithms for HDH systems with mass extraction and injections.

In general, better energy efficiency is obtained with components that have high effectiveness or low TTD. Both conditions require larger surface areas for the heat and mass transfer processes. To achieve the very high performance seen in some theoretical studies, impractically large components may be needed.

The on-design trends, at fixed component effectiveness, for varying operating conditions (e.g., top or bottom temperature) imply varying component size. Consequently, the off-design trends, for fixed component size, are somewhat different, as discussed in the next section.

9.2.2 Single-stage fixed-area HDH (off-design model)

The previous section evaluated the performance of the heat and mass exchangers by fixing their effectiveness or their pinch (TTD). This class of models can be very useful in comparing the performance of different cycle configurations or for assessing the performance of an HDH system under fixed operating conditions. However, these models cannot be used to compare different operating conditions for a given system because pinch and effectiveness are strong functions of the flow rates of the streams in the system. For example, when an extraction/injection is used to vary the operation of an HDH system, the effectiveness and pinch in each component will change and only the physical sizes of the components remain constant. Further, fixed pinch or effectiveness models do not specify the sizes of the exchangers used. In fact, if effectiveness is held constant while operating conditions change, the size of the equipment must in general be different for each operating point. Additionally, nothing guarantees that components having an arbitrary effectiveness or TTD can be efficiently designed and built.

Fully evaluating the performance of a specific HDH system requires fixing the size of the components and using transport models for the components under given operating conditions. We now discuss analysis of this type, following Chehayeb and co-workers [35, 36]. They modeled a water-heated closed-air open-water HDH system consisting of a packed-bed humidifier and a multi-tray bubble column dehumidifier, and they studied the effect of the air-to-water mass flow rate ratio (or HCR_d) on the performance of the system. The bubble column dehumidifier is modeled using the results of Tow and Lienhard [55, 56] for each of a series of 30 shallow trays. The packed-bed humidifier the Poppe and Rögener model [32] under the solution procedure of Kloppers and Kröger [33, 34]. Details of the component models and the solution procedures are in Chehayeb et al. [35, 36]. Here we focus on the major trends and conclusions.

9.2.2.1 Optimal performance of a single-stage system

Figure 9.12(a) shows the variation of the energy efficiency of the system represented by the gained output ratio, GOR, with the modified heat capacity rate ratio in the dehumidifier, HCR_d. It can clearly be seen that the best energy efficiency is achieved at $\mathrm{HCR}_d = 1$, or when the maximum change in the enthalpy rate is equal between the two interacting streams in the dehumidifier. This result is consistent with the fixed-effectiveness model reported by Narayan et al. [25]. In addition, we can see in Fig. 9.12(b) that the water production is also maximized when $\mathrm{HCR}_d = 1$.

This means that by fixing the size of the system, the top and bottom temperatures, and the feed flow rate, only one flow rate of air, or one mass flow rate ratio, maximizes both the energy efficiency and the water production. We can operate the system under different feed flow rates, but for each of these flow rates only one flow rate of air results in optimal performance in terms of both energy efficiency and water production. As we increase the feed flow rate, the water production rate will increase but the energy efficiency will drop because the area per unit flow will decrease and so will the effectiveness of the exchangers. The trade-off between the different values of the feed flow rate is then between energy efficiency and water production. Assessing that trade-off requires a cost analysis.

9.2.2.2 Relationship of $\mathrm{HCR}_d = 1$ to entropy generation minimization

To understand why HCR_d is an important parameter when looking at the energy efficiency of the system, we consider the entropy generated per unit product. Figure 9.13 shows the entropy generated in the dehumidifier and the humidifier separately and collectively for different values of the mass flow rate ratio. The total entropy generated is minimized at $\mathrm{HCR}_d = 1$, which explains why energy efficiency is highest at that mass flow rate ratio. This result is consistent

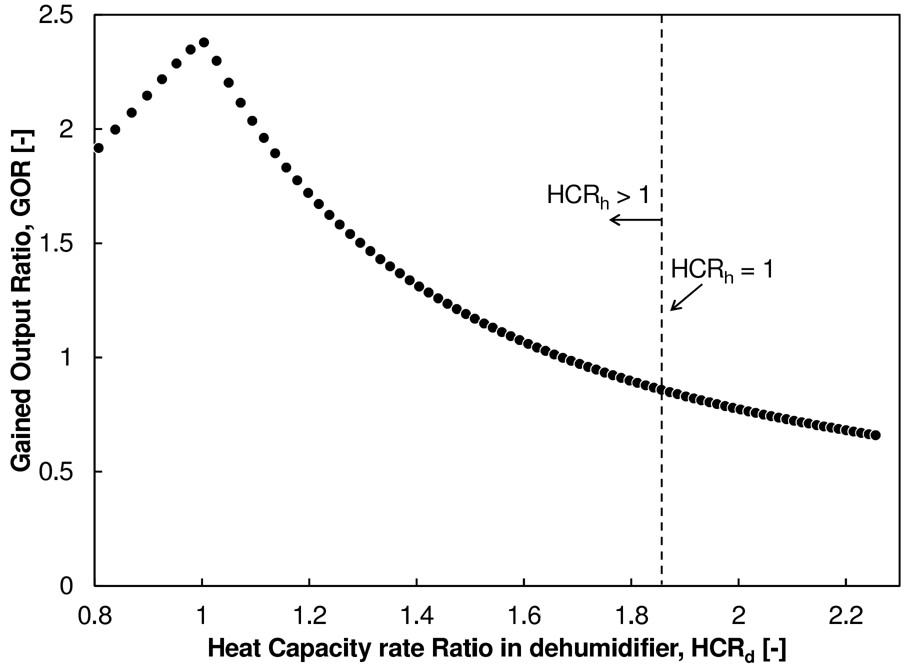

(a) Variation of GOR with HCR$_d$.

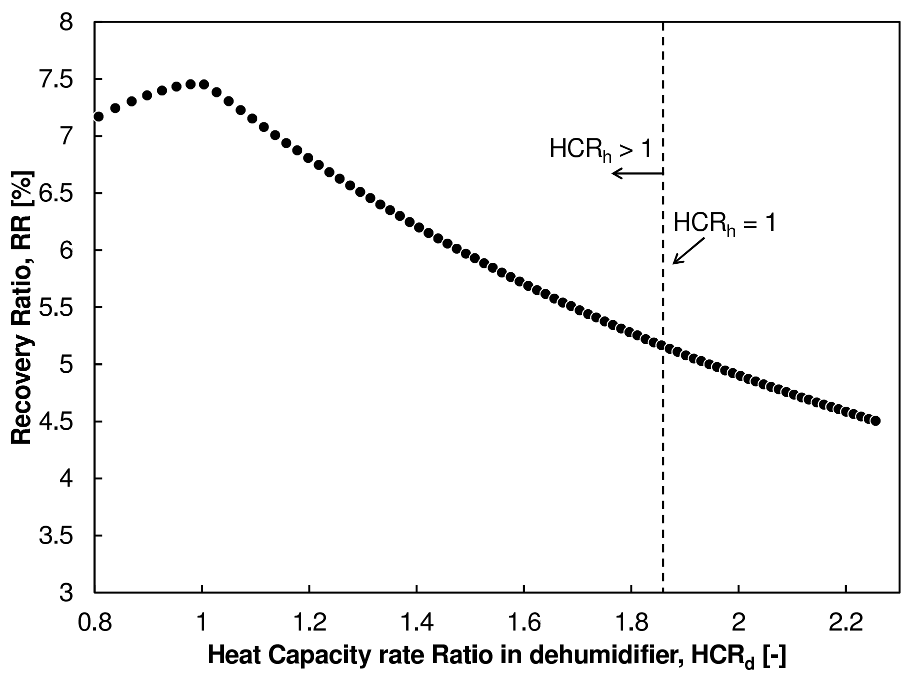

(b) Variation of RR with HCR$_d$.

Figure 9.12: Variation of the performance of a single-stage HDH system with HCR$_d$ [36].

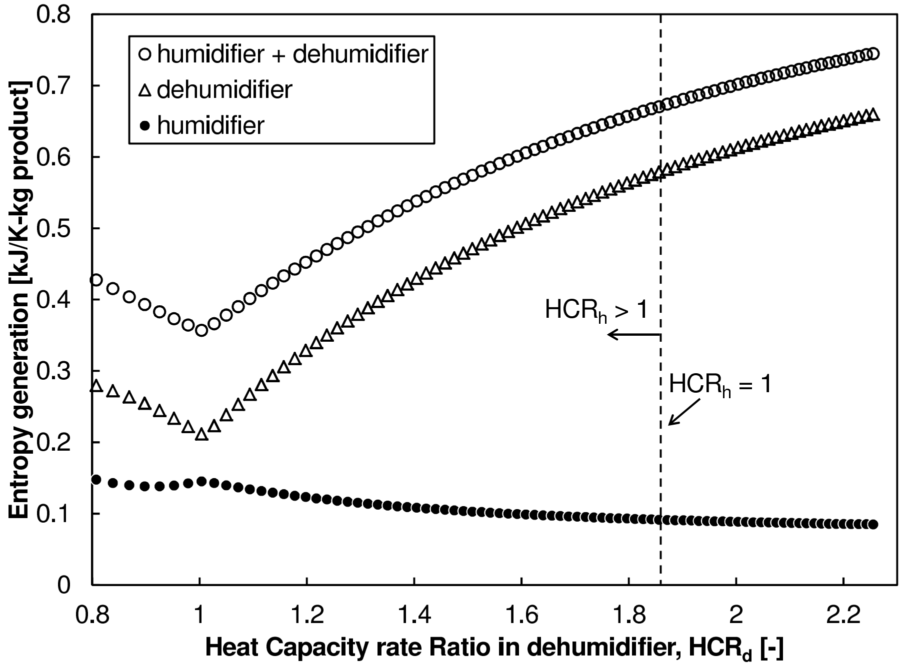

Figure 9.13: Variation of entropy generation with HCR$_d$ [36].

with the conclusion by Mistry et al. [21] that the best performance is achieved when the specific entropy generated is minimized.

The entropy generated in the dehumidifier is always larger than that generated in the humidifier, which is almost independent of HCR$_d$. Further, the entropy generated in the dehumidifier is minimized at HCR$_d$ = 1 whereas the entropy generated in the humidifier shows no change in trend around HCR$_h$ = 1. What can be concluded from this graph is that the variation of the mass flow rate ratio affects the entropy generated in the dehumidifier much more strongly than that generated in the humidifier, as evident from the slopes of the two curves in Fig. 9.13. For this reason, HCR$_d$ is the parameter to monitor when thermodynamically balancing a single-stage HDH system. Balancing the dehumidifier from a control volume perspective has little negative effect on the humidifier, and therefore serves to maximize the performance of the system.

In a heat and mass exchanger, entropy generation can be ascribed to two factors: (1) a finite mean driving force for heat and mass transfer; and (2) a spatial or temporal variance in the driving force [57]. The size of the system affects mainly the mean driving force whereas the mass flow rate ratio affects mostly the variance of the driving force. In this study, in order to better show the effect of the mass flow rate ratio, a very large system was modeled ($\varepsilon_d \approx 99\%$, $\varepsilon_h \approx 95\%$). In a large system, the total entropy generation is smaller; and the entropy generation due to the variance of the driving forces forms a greater fraction of the total entropy generation, so that the effect of balancing more pronounced. Similar but less pronounced results are found in smaller systems.

We can also look at the effect of the mass flow rate ratio on the driving forces for heat and mass transfer. The averages and variances in this study are weighted spatially using the surface area. Figure 9.14(a) shows the variation of the average driving force for heat transfer, namely the temperature difference between the two interacting streams in the humidifier and the dehumidifier. Both are maximized at $\mathrm{HCR}_d = 1$, which means that, given a fixed exchanger size and relatively fixed heat transfer coefficients, the highest heat duty is achieved at $\mathrm{HCR}_d = 1$. For smaller systems, the curves shown in Fig. 9.14(a) become much flatter, and the peak in the dehumidifier remains at $\mathrm{HCR}_d = 1$ whereas that in the humidifier shifts to HCR_d slightly larger than 1.

Figure 9.14(b) shows the variation of the average difference in relative humidity in both the humidifier and dehumidifier. The difference is taken between the humidity ratio of air and the humidity ratio at saturation evaluated at the temperature and salinity of the water at multiple locations along the exchangers. The average difference in the humidity ratio in the dehumidifier is maximized whereas that in the humidifier is close to its maximum at $\mathrm{HCR}_d = 1$.

Figure 9.15 shows the variation of the variances of the stream-to-stream temperature and humidity ratio differences with HCR_d. At $\mathrm{HCR}_d = 1$, the variance of the temperature difference in the dehumidifier is minimized and that in the humidifier is close to its minimum. In addition, the variance of the humidity ratio difference in the dehumidifier is minimized and only the variance of the humidity ratio difference in the humidifier is not at a minimum at $\mathrm{HCR}_d = 1$. In the dehumidifier, the minimum variance of the temperature difference shifts to HCR_d slightly larger than 1 whereas the variance of the humidity ratio difference shifts to HCR_d less than 1. Balancing the two driving forces can be done by operating the system around $\mathrm{HCR}_d = 1$.

Minimizing the variance of the driving force means that it remains as close as possible to its average along the heat and mass exchanger. This in turn means that the driving force will not become too large at some points and too small at other points, so that all of the available exchanger surface area is used fully. If the heat and mass exchanger is not balanced properly, the stream with the smaller total heat capacity rate will quickly reach a state close to that of the other stream, and the rest of the available area will only result in a small heat duty because the driving force is too small. This result is consistent with the conclusion reached by Thiel et al. [57] that the best performance is obtained by minimizing the variance of the driving force.

9.2.2.3 Variation of GOR with top temperature

Chehayeb et al. [35] examined the effect of top and bottom temperatures on GOR, RR, and HCR_d considering both fixed and variable mass flow rate ratios. Figure 9.16(a) shows the variation of the GOR of two systems with the top temperature. The first system is designed to operate between 25 °C and 90 °C, so has $m_r = 4.2$ to get $\mathrm{HCR}_d = 1$ at 25 °C and 90 °C. But as the top temperature varies, m_r is kept constant, so the performance of the system drops. The second system is a dynamic system that adjusts its m_r such that HCR_d is always equal to unity. The performance is more stable, and in fact, when the top temperature drops, the energy efficiency of the dynamic system actually increases slightly. The effect of dynamic control on recovery ratio was much lower [Fig. 9.16(b)]. In addition, the effect of the top temperature on performance is much larger than that of the bottom temperature.

The difference between the passive and dynamic system is very important if the HDH system relies on a heating source, such as solar power, that fluctuates. Active control is clearly highly beneficial. If a control system is not feasible, the system should be designed by taking into consideration the variation of the top temperature, and should operate at the m_r that maximizes

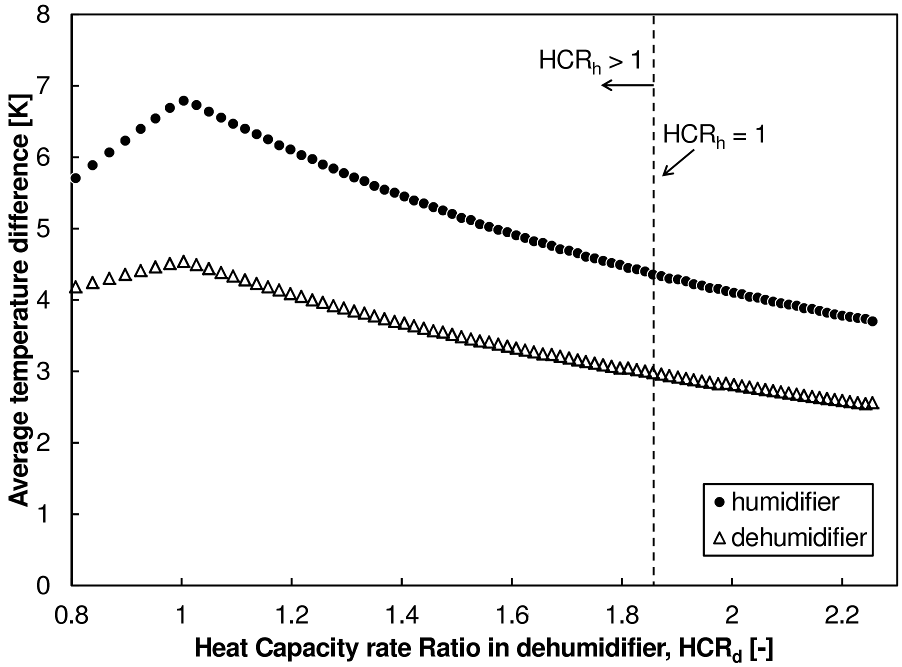

(a) Variation of the average of the stream-to-stream temperature difference with HCR$_d$.

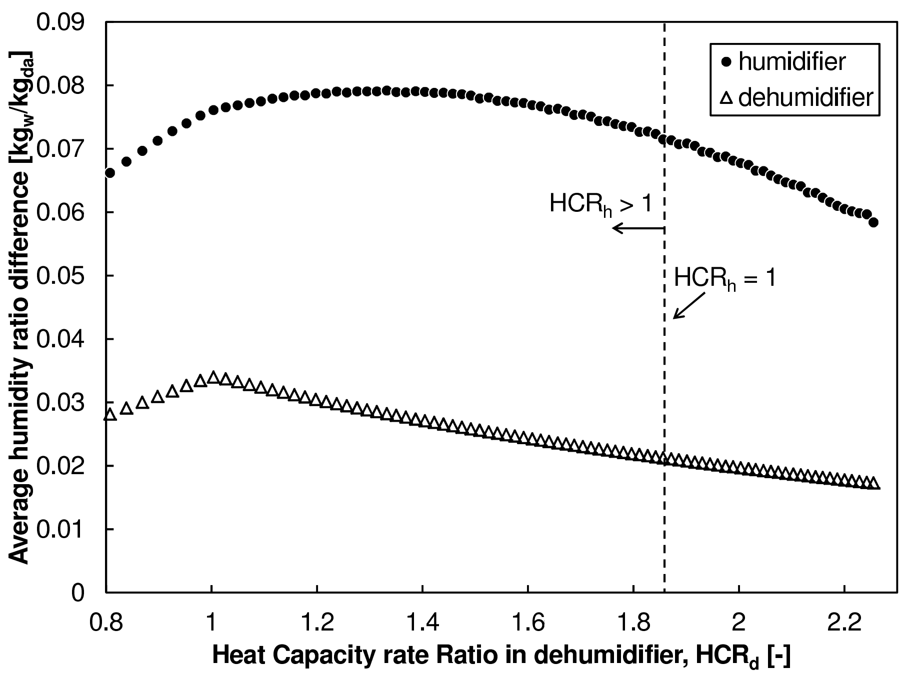

(b) Variation of the average of the stream-to-stream humidity ratio difference with HCR$_d$.

Figure 9.14: Variation of the average of the driving forces with HCR$_d$ [36].

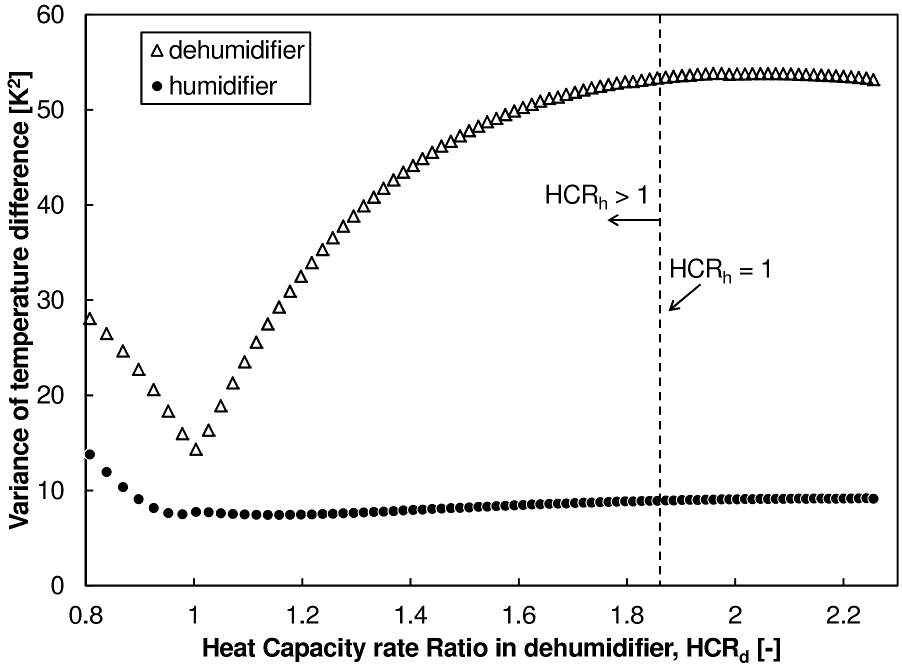

(a) Variation of the variance of the stream-to-stream temperature difference with HCR$_d$.

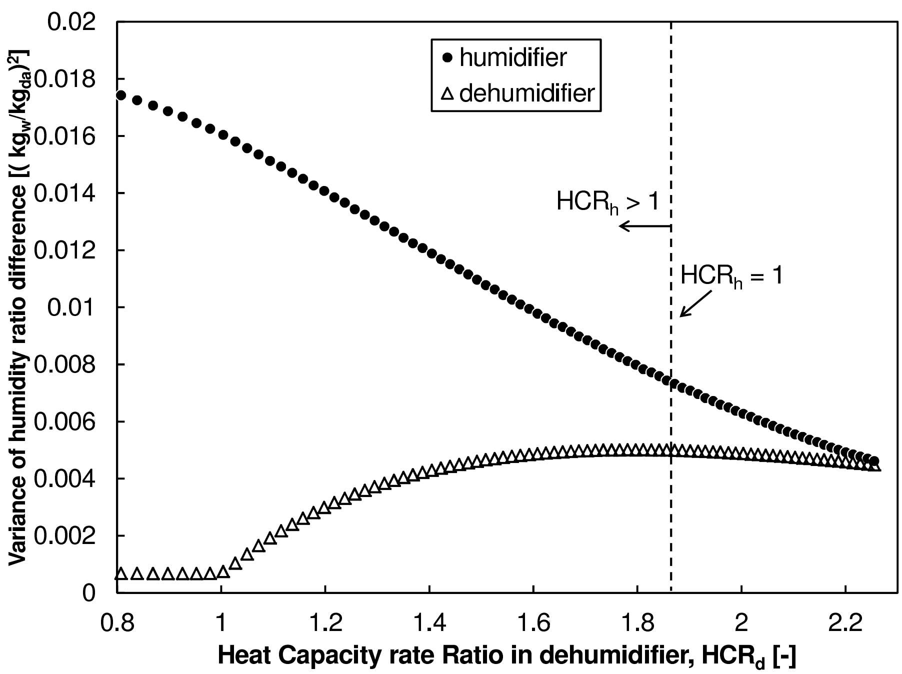

(b) Variation of the variance of the stream-to-stream humidity ratio difference with HCR$_d$.

Figure 9.15: Variation of the variance of the driving forces with HCR$_d$ [36].

the total output over a certain period of time.

Passive control strategies for solar heating have also been explored. Summers et al. [58] designed and tested air heating solar collectors that incorporated phase-change materials to stabilize the top temperatures. By embedded a wax below the absorber plate, they limited the peak air temperature by the wax melting-point temperature. Further, as solar radiation declined late in the day, the wax refroze, giving up its latent heat and keeping the air temperature stable. These systems incorporated roughened absorber plates to enhance heat transfer [59].

9.2.2.4 Summary of off-design findings

1. Thermodynamically balancing an HDH system, which is done by setting $\mathrm{HCR}_d = 1$, maximizes energy efficiency and water recovery. The effect on energy efficiency is much greater than that on water recovery ratio.

2. Setting $\mathrm{HCR}_d = 1$ minimizes the entropy generation per unit product by minimizing the variances in the driving forces to heat and mass transfer. This results in the best use of the available surface area in the heat and mass exchangers.

3. Active control to hold $\mathrm{HCR}_d = 1$ is highly beneficial.

4. HCR_h is not a useful parameter for system performance.

5. Top temperature has a greater effect on system performance than bottom temperature.

9.3 Systems with Mass Extraction and Injection

As discussed in Section 9.1.3, the use of mass extractions and injections to vary the water-to-air mass flow rate ratio in the humidifier and the dehumidifier can help in reducing entropy production in those devices and raising the cycle's GOR [25]. A comprehensive method of thermodynamic analysis is available for the design of mass extractions and injections in the HDH system [28, 29, 31]. This approach draws upon the fundamental observation that there is a single value of water-to-air mass flow rate ratio (for any given boundary conditions and component effectivenesses) at which the system performs optimally [17, 25, 31, 36].

A schematic diagram of a representative the HDH system with mass extractions and injections is shown in Figure 9.17. The system shown is a water-heated, closed-air, open-water system with three air extractions from the humidifier into the dehumidifier. States a to d are used to represent various states of the seawater stream and states e and f represent that of moist air before and after dehumidification. Several other embodiments of the system are possible based on the various classifications of HDH listed earlier in this chapter.

Enthalpy Pinch Model McGovern et al. [28] proposed that it is advantageous to normalize enthalpy rates by the amount of dry air flowing through the system for easy representation of the thermodynamic processes in enthalpy versus temperature diagrams (see Figure 9.18). We use this concept here and derive the following equation from Eq. (9.7) by dividing the numerator

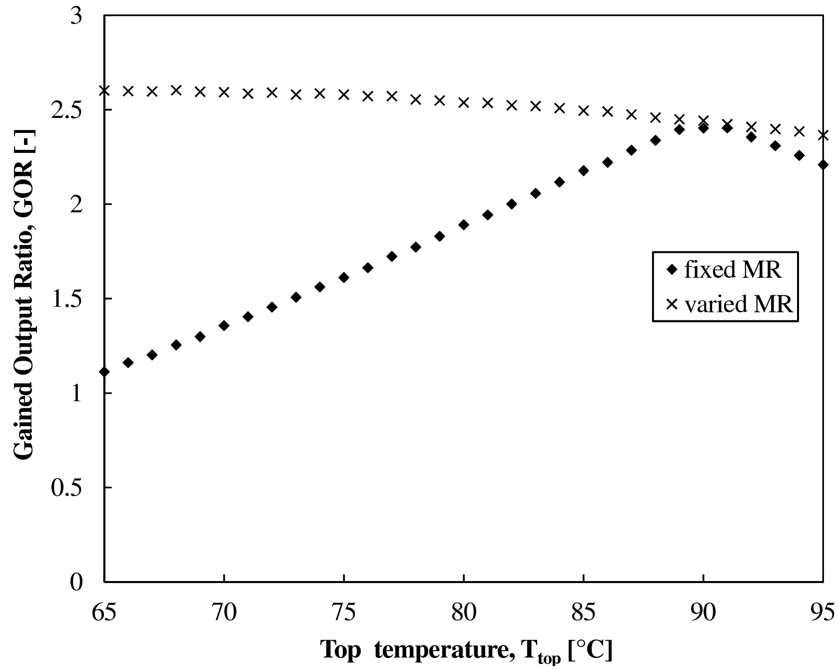

(a) Variation of GOR with top temperature.

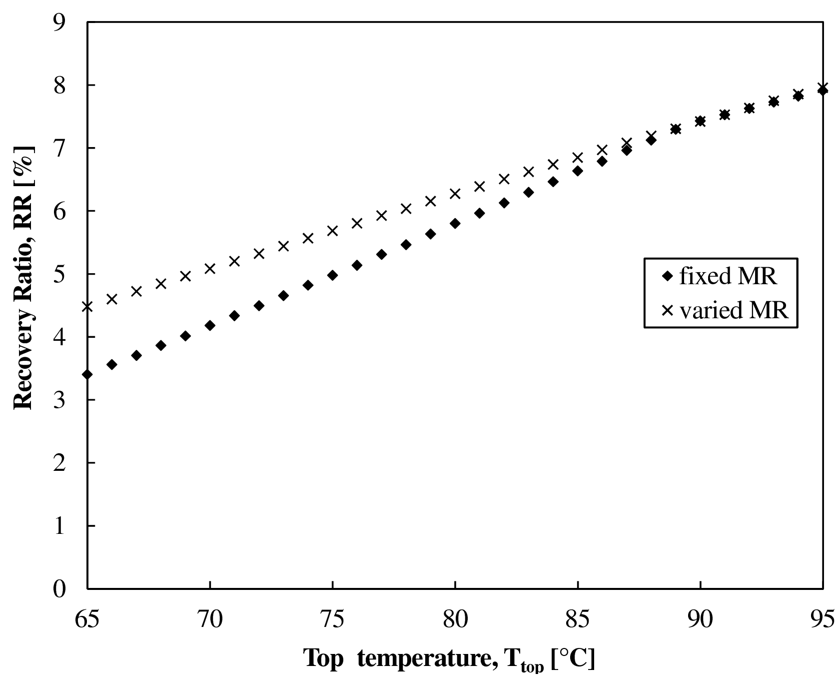

(b) Variation of RR with top temperature.

Figure 9.16: Effect of top temperature on performance for fixed or variable mass flow rate ratio, m_r [35].

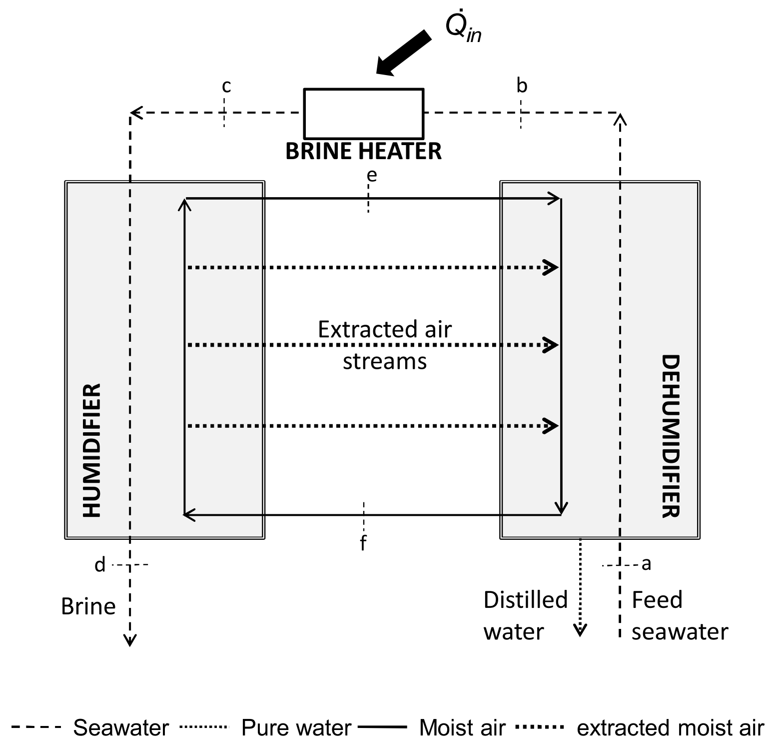

Figure 9.17: Schematic diagram of a water-heated, closed-air, open-water humidification-dehumidification desalination system with mass extraction and injection of the moist air stream [29].

and the denominator by the mass flow rate of dry air ($\dot{m}_{da}$) to obtain an expression in terms of the enthalpy per unit mass of dry air, h^*:

$$\varepsilon = \frac{\Delta h^*}{\Delta h^*_{\max}} \tag{9.10}$$

$$= \frac{\Delta h^*}{\Delta h^* + \Psi_{TD}} \tag{9.11}$$

Ψ_{TD} is the loss in enthalpy rates at terminal locations because of having a "finite-sized" HME device, and it is defined by the minimum of two values as follows:

$$\Psi_{TD} = \min\left(\frac{\Delta \dot{H}_{\max,c}}{\dot{m}_{da}} - \Delta h^*, \frac{\Delta \dot{H}_{\max,h}}{\dot{m}_{da}} - \Delta h^*\right) \tag{9.12}$$

$$= \min\big(\Psi_c, \Psi_h\big) \tag{9.13}$$

In the case of a heat exchanger, Ψ_{TD} will be analogous to the minimum terminal stream-to-stream temperature difference (TTD). TTD is seldom used to define performance of a heat exchanger in thermodynamic analyses; the temperature pinch is the commonly used parameter. The difference is that pinch is the minimum stream-to-stream temperature difference at any point in the heat exchanger and not just at the terminal locations. Like temperature pinch, Ψ

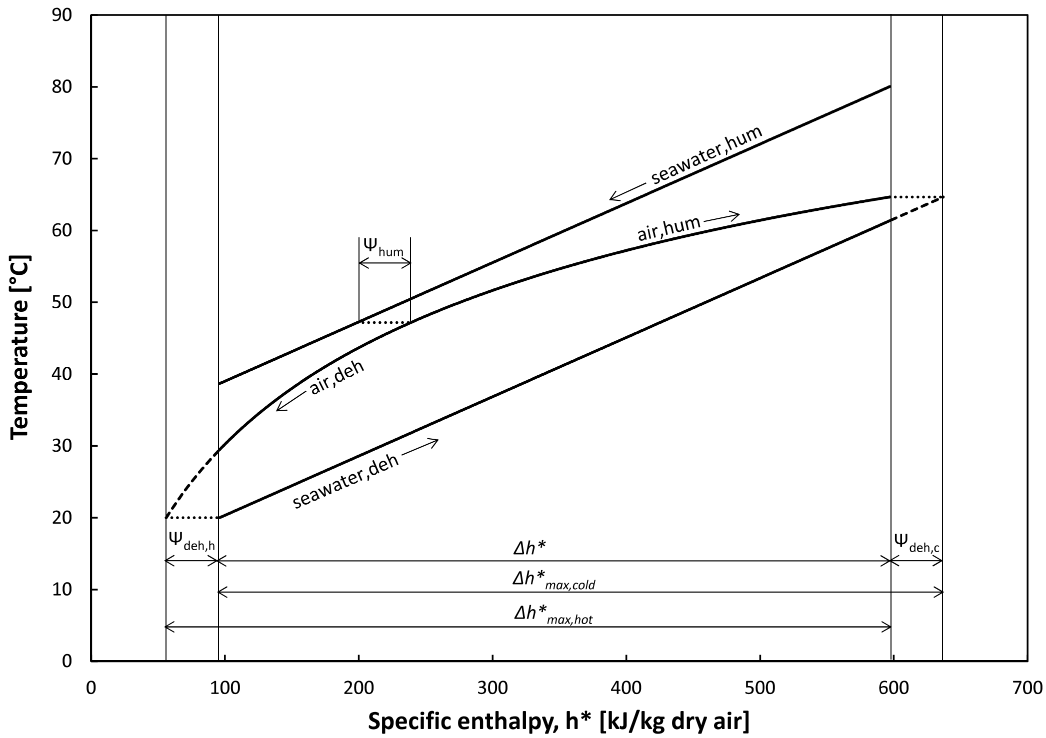

Figure 9.18: Temperature-enthalpy profile of a balanced single-stage system with feed at $T_a = 20$ °C, a top brine temperature $T_c = 80$ °C, and $\Psi_{\text{hum}} = \Psi_{\text{deh}} = 20$ kJ/kg dry air [29].

can be defined as the minimum loss in enthalpy rate due to a finite device size at any point in the HME device and not just at the terminal locations. Thus, the general definition of Ψ will be as follows:

$$\Psi = \min_{\text{local}}\left(\Delta h^*_{\text{max}} - \Delta h^*\right) \tag{9.14}$$

Hence, based on the arguments presented in this section, we can say that Ψ for an HME device is analogous to temperature pinch for a heat exchanger, and it can be called the 'enthalpy pinch'. In view of the presence of the concentration difference as the driving force for mass transfer in HME devices, a temperature pinch or a terminal temperature difference should not be used when defining the performance of the device. Further details about the enthalpy pinch and its significance in thermal design of HME devices are given in Reference [29]. Balancing of HDH cycles has been studied in further detail in References [30, 31, 36, and 60].

9.3.1 System Balancing Algorithms (On-Design Model)

The concepts of thermodynamic balancing developed for HME devices have been applied to HDH system designs that use extraction and injection [29, 31]. Detailed algorithms for systems with zero, single, and multiple extractions have been developed. Temperature-enthalpy diagrams were used to model the systems, and the relevant conservation laws were applied. Figure 9.19 illustrates temperature versus enthalpy of a system with a single extraction and

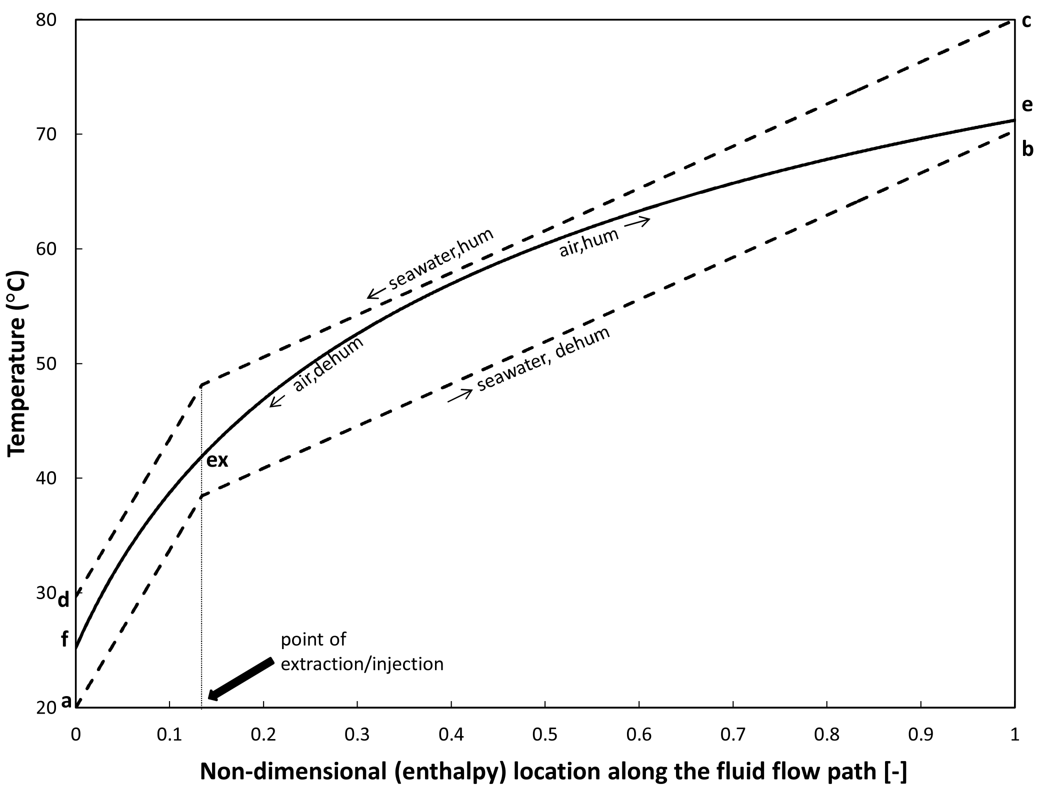

Figure 9.19: Temperature profile representing the HDH system with a single extraction. Boundary conditions: $T_a = 20$ °C; $T_c = 80$ °C; $\Psi_{\text{deh}} = \Psi_{\text{hum}} = 20$ kJ/kg dry air [29].

injection. In the illustrated case, the air was extracted from the humidifier at the state 'ex' and injected in a corresponding location in the dehumidifier with the same state 'ex' to avoid generating entropy during the process of injection. This criteria for extraction is applied for all the cases reported in this paper since it helps us study the effect of thermodynamic balancing, independently, by separating out the effects of a temperature and/or a concentration mismatch between the injected stream and the fluid stream passing through the HME device (which when present can make it hard to quantify the reduction in entropy generated due to balancing alone). The physical location of extraction (and the size of components) is not determined by on-design models; off-design (fixed area) models are required, as discussed in Section 9.3.2.

The effect of the number of extractions (at various enthalpy pinches) on the performance of the HDH system is shown in Figure 9.20. Several important observations can be made from this chart.

First, the increase of GOR through extraction/injection is more significant for smaller enthalpy pinch. Beyond Ψ of 25 to 30 kJ/kg dry air, little or no benefit is obtained. Second, the benefit increases steadily as $\Psi \to 0$, i.e., for larger effectiveness or larger heat transfer area. Third, the number of extractions that can be used to increase GOR rises as Ψ decreases. In generating this figure, the temperature required at the locations of extraction and injection was determined, as was the appropriate mass flow rate to be transferred. The optimal temperature

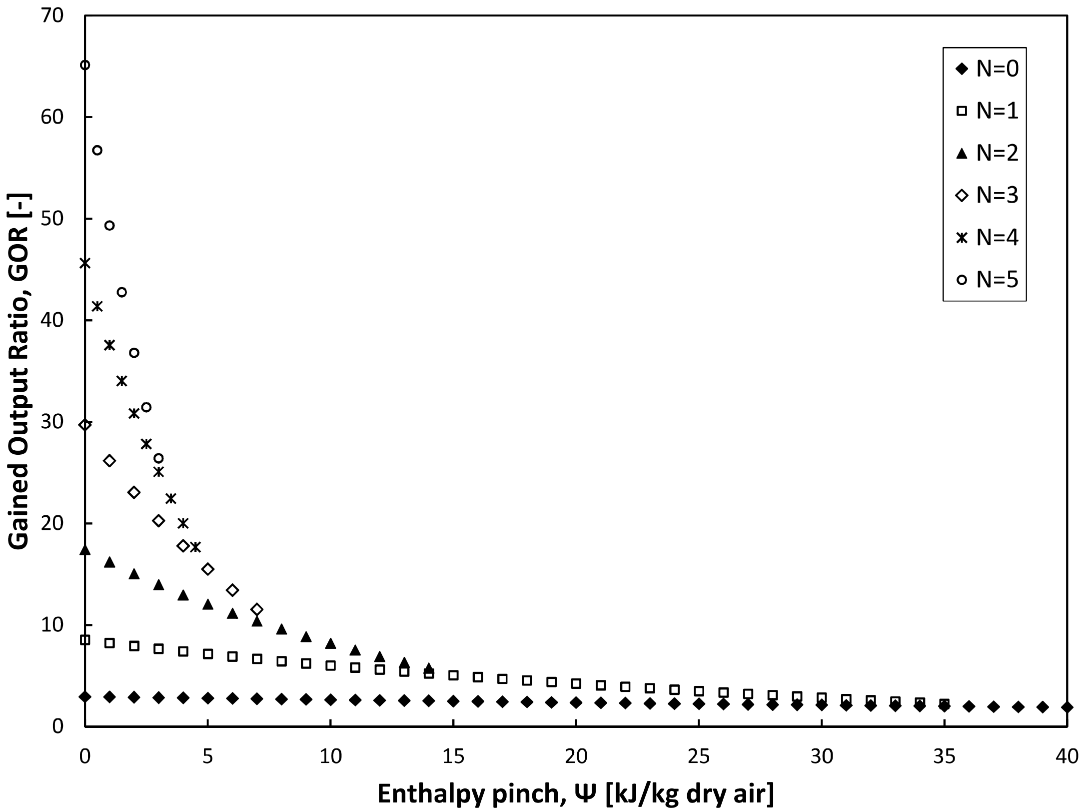

Figure 9.20: Variation of GOR with enthalpy pinch, Ψ, and number of extractions, *N*. Boundary conditions: $T_a = 20$ °C, $T_c = 80$ °C [31].

of the extracted/injected air stream decreased as enthalpy pinch increased and as the number of extractions increased. The appropriate mass flow rate ratio in each stage was also found.

Narayan et al. [29] discussed the concept of continuous extraction (an infinite number of infinitesimal extractions), which in the present case leads to GOR = 109 at $\Psi = 0$, a system of infinite area. Chehayeb et al. [31] showed that for $\Psi > 0$, a finite number of extractions gives higher GOR than does continuous extraction. Chehayeb et al. also showed that balancing by extraction/injection has a much greater effect on energy efficiency (GOR) than on the water recovery ratio.

9.3.2 Balancing fixed-area systems by extraction/injection (off-design analysis)

Chehayeb et al. [36] extended the single-stage HDH analysis described in Section 9.2.2 to systems using a single air extraction/injection. They studied a fixed size system in which the location of extraction/injection was adjusted to obtain the optimal temperature for the extracted/injected stream. For example, in the 30 tray bubble column dehumidifier, number of trays in the first and second stages was varied to match this temperature (e.g., perhaps with 12 trays in the first stage and 18 in the second, etc.).

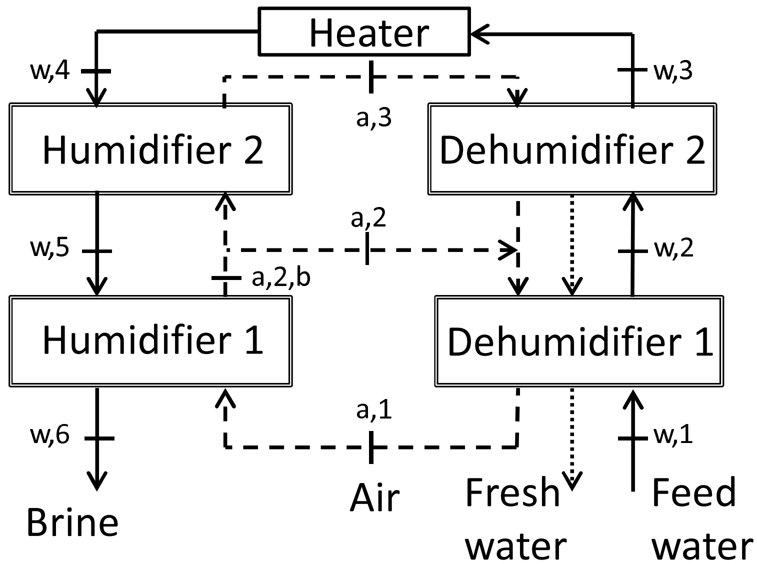

Figure 9.21: Water-heated, closed-air, open-water HDH system with a single extraction [36].

Each stage has a separate value of HCR_d, denoted $\mathrm{HCR}_{d,1}$ and $\mathrm{HCR}_{d,2}$ (see Fig. 9.21). In a balanced condition, $\mathrm{HCR}_{d,1} = \mathrm{HCR}_{d,2} = 1$. Figures 9.22 and 9.23 show GOR as a function the two HCR_d's. Figure 9.24 shows the corresponding relationship of GOR with RR. The highest GOR reached in this system without extraction/injection was 2.4. This value was raised 58% to 3.8 using a single extraction/injection. In the same case, RR was increased from 7.7% to 8.2%. The optimal performance in this case was achieved when the area of the dehumidifier was equally divided between the two stages. As for the single stage system, HCR_h was an irrelevant parameter in balancing.

Chehayeb et al. also showed that it is always better to extract from the humidifier and inject in the dehumidifier, and that it is better not to extract than to extract in the opposite direction. This result is true for either an air or a water extraction. They further explained some contradictory findings in an earlier study of extraction [60, 61]. Finally, they noted that having the proper physical location of extraction/injection is essential to reaching a balanced condition.

9.3.3 Experimental realization of HDH with and without extraction/injection

A pilot-scale HDH unit with a peak production capacity of 700 L/day was constructed and detailed experiments were performed [30]. Those experiments validated the theories discussed thus far. The experimental system comprised a packed bed humidifier and high-performance polypropylene plate-and-tube dehumidifiers, configured in a closed-air, open-water, water-heated cycle (cf. Fig. 9.4).

Experiments without extraction showed that as either mass flow rate ratio, m_r, or feed water temperature (bottom temperature) was varied, the GOR reached a maximum when $\mathrm{HCR}_d = 1$,

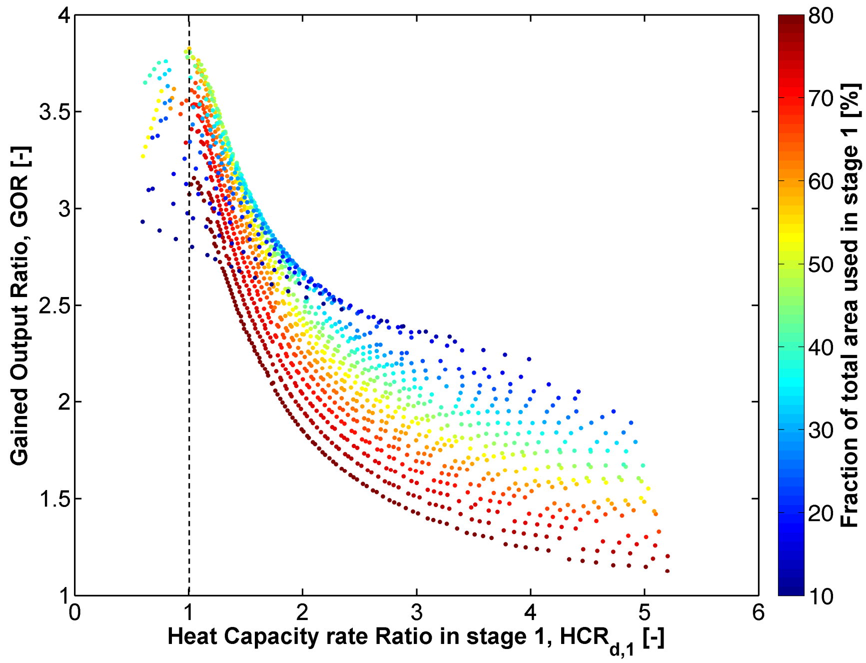

(a) Variation of GOR with HCR$_{d,1}$.

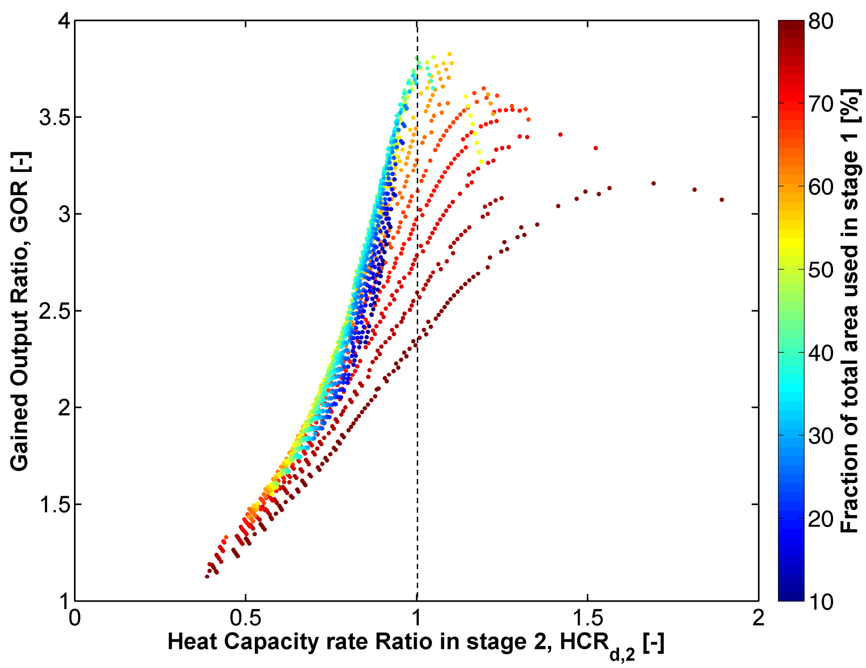

(b) Variation of GOR with HCR$_{d,2}$.

Figure 9.22: Variation of GOR with HCR$_{d,1}$ and HCR$_{d,2}$ [36].

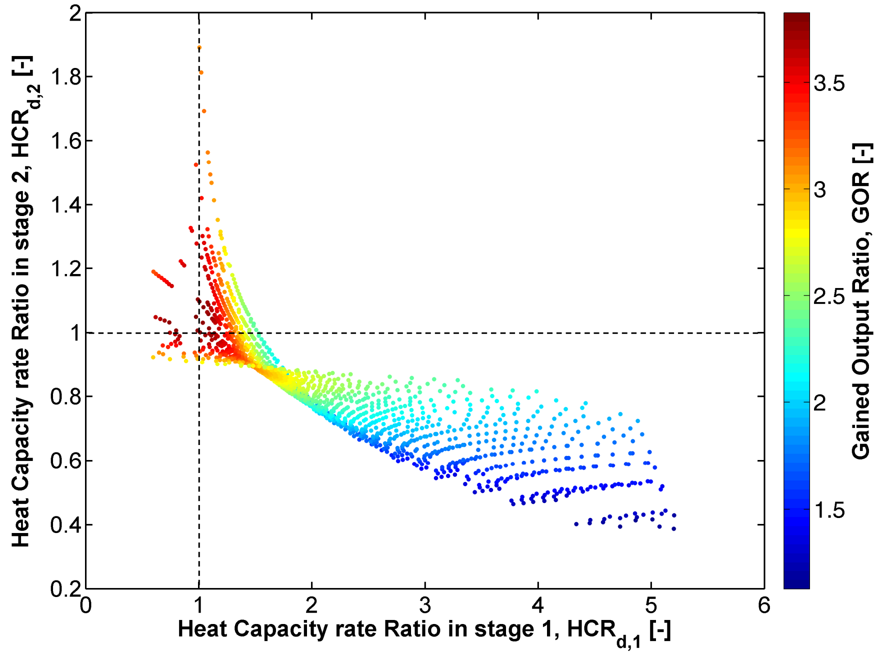

Figure 9.23: Variation of GOR with $HCR_{d,1}$ and $HCR_{d,2}$ [36].

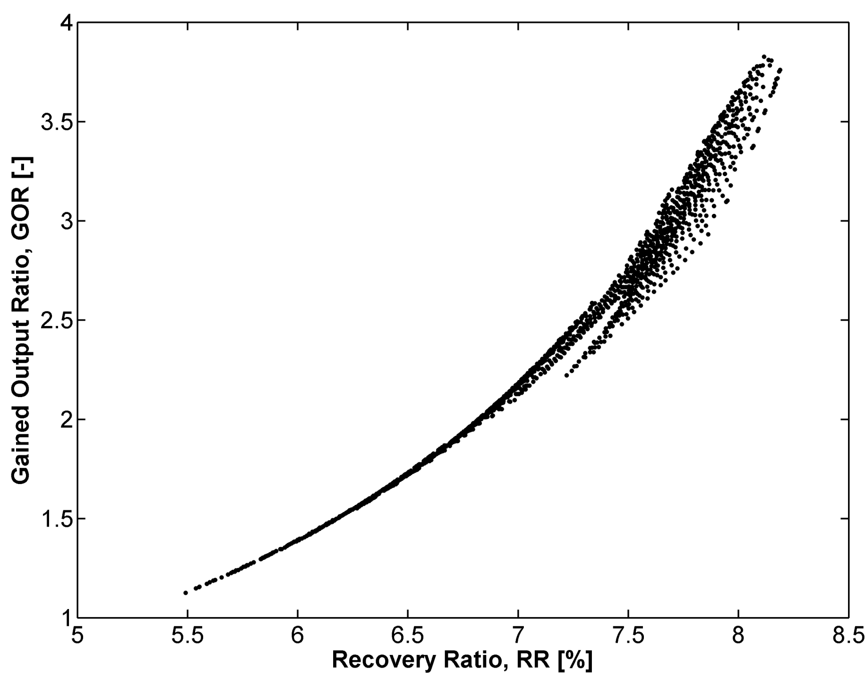

Figure 9.24: Variation of GOR with RR [36].

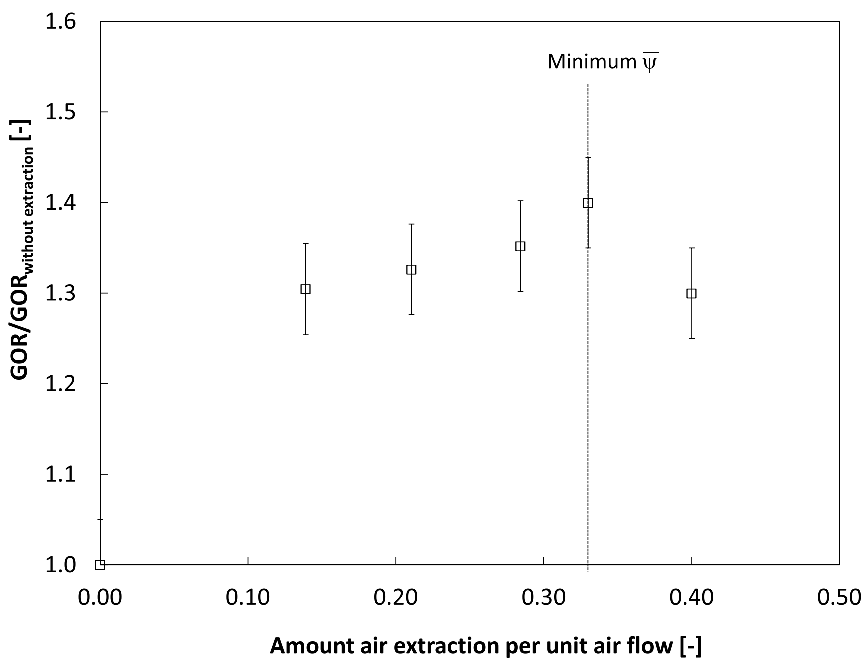

Figure 9.25: Effect of mass flow rate of air extracted on the performance of the HDH system. Boundary conditions: $T_a = 25$ °C; $T_c = 90$ °C; $N = 1$ [30].

very much as seen from the modeling result in Figs. 9.12(a). The measured entropy generation was also minimized at the balanced condition (cf. Fig. 9.13). When the top temperature was varied while holding $\text{HCR}_d = 1$, the GOR increased with top temperature, rising by 80% from 60°C to 90°C. This off-design behavior should be contrasted to the on-design behavior (Figs. 9.8 and 9.9). which show GOR to drop as top temperature rises. When HDH components are modeled as fixed effectiveness (on-design), the size of the components increases or decreases with a change in boundary conditions. For example, at a lower top temperature, a component effectiveness of 80% will need a much larger component than for a higher top temperature. For this reason, off-design performance does not follow the trend suggested by on-design models.

When operating between 25°C and 90°C, the system without extraction had a measured GOR of 2.6. With a single extraction at optimal conditions, the GOR rose to 4.0 (with experimental uncertainty of ±5%), an enhancement of 54%. At optimal operation, this system had an enthalpy pinch $\Psi = 19$ kJ/kg dry air. Numerical modeling of the same system by Chehayeb et al. [36] produced a GOR of 2.3 without extraction (11% difference) and 4.7 with extraction (17% difference). Heat loss to the environment in the experimental system and some simplifications in the model account for these differences, as discussed in [36]. The effect of varying the extracted mass flow rate around the optimum condition is shown in Fig. 9.25.

9.3.4 Summary of HDH characteristics related to extraction/injection

1. Thermodynamic balancing of an HDH system, with $\text{HCR}_d = 1$, maximizes GOR and water recovery. This condition also minimizes entropy generation per unit product water.

2. A higher top temperature will increase the GOR of an HDH system of specified size.
3. Extraction/injection can raise the energy efficiency and water recovery. This process effectively divides the system into multiple stages. The objective of extraction/injection is to obtain $\mathrm{HCR}_d = 1$ in each dehumidifier stage.
4. A single air extraction can raise the GOR of a closed-air, open-water, water-heated cycle by more than 50%.
5. Extraction should always be from the humidifier with injection into the dehumidifier, and it is better not to extract than to extract in the opposite direction. This result is true for either an air or a water extraction.
6. The physical location of extraction/injection is essential. An off-design analysis is required to determine the proper positions.
7. Thermodynamic balancing by extraction/injection raises GOR only when the enthalpy pinch is sufficiently low, $\Psi \lesssim 25$ to 30 kJ/kg dry air. Using more than one extraction is only beneficial for even lower Ψ, less than about 15. Only components of high effectiveness can reach such low values of Ψ, and the increase in energy efficiency may not justify the associated increase in capital cost.

9.4 Bubble Column Dehumidification

When a non-condensable gas is present, the thermal resistance to condensation of vapor on a cold surface is much higher than in a pure vapor environment. This increase is, primarily, caused by the diffusion resistance to transport of vapor through the mixture of non-condensable gas and vapor. Many researchers have previously examined this effect [62–70]. When even a few mole percent of non-condensable gas are present in the condensing vapor, the deterioration in the heat transfer rates can be up to an order of magnitude [71–76]. From experimental reports in literature, the amount of deterioration in heat transfer is a very strong (almost quadratic) function of the mole fraction of non-condensable gas present in the condensing vapor.

In HDH systems, a large percentage of air (60–90% by mass) is present by default in the condensing stream. As a consequence, the heat exchanger used for condensation of water out of an air-vapor mixture (i.e., the dehumidifier) has very low heat and mass transfer rates (an 'equivalent' heat transfer coefficient as low as 1 W/m^{2}K in some cases [14, 77–79]). This leads to very high heat transfer area requirements in the dehumidifier (up to 30 m^2 for a 1 m^2/day system). In this section, we describe how to achieve a substantial improvement in the heat transfer rate by condensing the vapor-gas mixture in a column of cold liquid, rather than on a cold surface, by using a bubble column heat and mass exchanger.

In a bubble column dehumidifier, moist air is sparged through a porous plate (or any other type of sparger [80]) to form bubbles in a pool of cold liquid. The upward motion of the air bubbles causes a wake to be formed underneath the bubble which entrains liquid from the pool, setting up a strong circulation current in the liquid pool [81]. Heat and mass are transferred from the air bubble to the liquid in the pool in a direct contact transport process. At steady state, the liquid, in turn, loses the energy it has gained to a coolant circulating through a coil placed

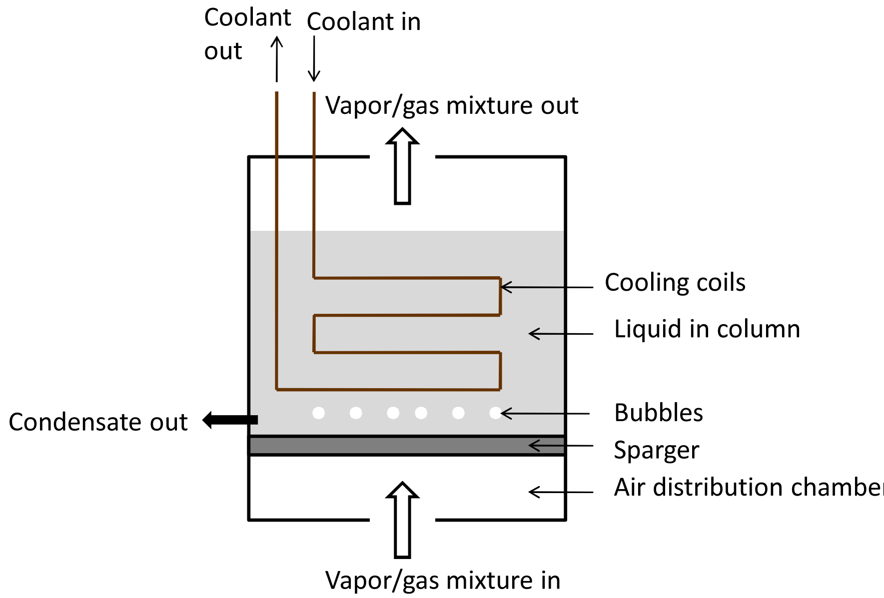

Figure 9.26: Schematic diagram of the bubble column dehumidifier [82].

in the pool for the purpose of holding the liquid pool at a steady temperature. The system is illustrated in Figure 9.26, as was first proposed by Narayan et al. [82]. In an HDH system, the "coolant" would be the saline feed water, which becomes preheated as it moves through the bubble column, similar to Figure 9.1.

9.4.1 Modeling and Experimental Validation

A thermal resistance models for the condensation of water from an air-vapor mixture in a bubble column heat exchanger were introduced in Reference [82] and have been revised and refined in References [55, 56, 83, 84]. The primary temperatures in the resistance network are: (1) the average local temperature of the air-vapor mixture in the bubbles (T_{air}); (2) the average temperature of the liquid in the pool (T_{column}); and (3) the average local temperature of the coolant inside the coil ($T_{coolant}$). Between T_{air} and T_{column} heat and mass transfer occurs by direct contact. The liquid pool is well-mixed by the bubbles, and may be considered to hold a constant temperature. The local heat transfer from the pool to the coolant can be represented by heat transfer coefficients inside and outside the coil, and the temperature change of the coolant can be modeled as a single-stream heat exchanger. The heat transfer between the moist air stream may be modeled similarly. Experimental support for the models is very strong [55, 82, 84]. The heat transfer coefficients between the liquid column and the coil surface, in particular, can be very large, in the range of 5,000 W/m^{2}K [84].

9.4.2 Multistage Bubble Column Dehumidifiers

In an HDH system, the nearly isothermal state of the liquid in the bubble column dehumidifier reduces the temperature to which feedwater can be preheated in the coils. This limits the

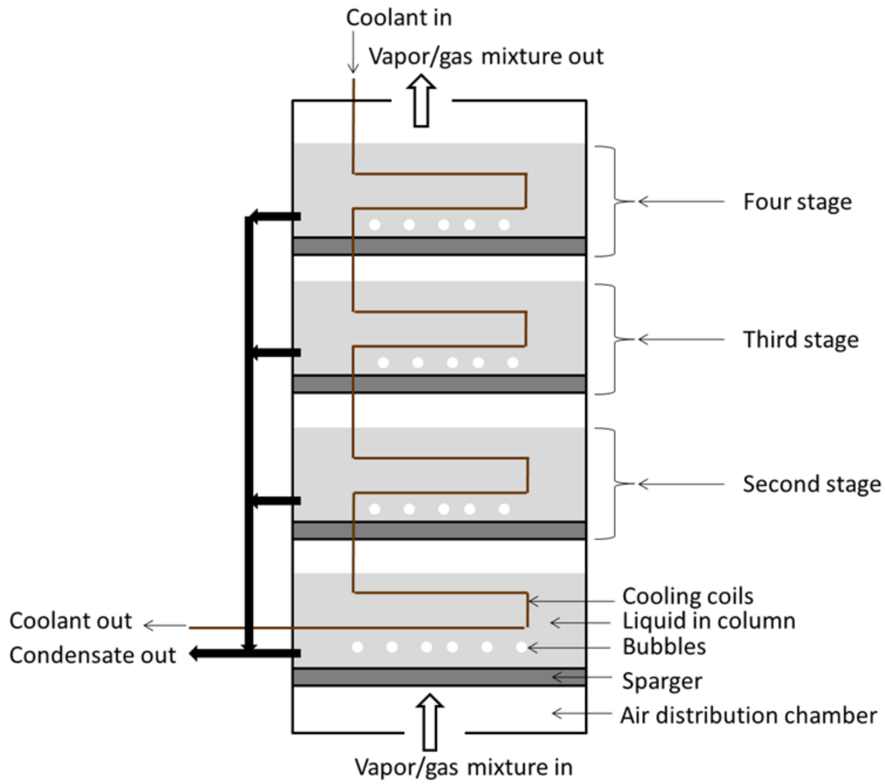

Figure 9.27: Schematic diagram of multi-stage bubble column dehumidifier [3].

energy effectiveness of the device [38]. A low effectiveness in the dehumidifier, reduces the HDH system performance significantly [17, 55]. In this section, we detail an innovation which increases the energy effectiveness of these devices [17, 35, 85-90].

A schematic diagram of a multi-stage bubble column is shown in Figure 9.27. In this device, the moist air is sparged successively from the bottom-most (first) stage to the top-most (last) stage through pools of liquid in each stage. The coolant enters the coil in the last stage and passes through the coil in each stage and leaves from the first stage. Thus, the moist air and the coolant are counter-flowing from stage to stage. The condensate is collected directly from the column liquid in each stage.

Figure 9.28 illustrates the temperature variations in a single-stage and multistage bubble column [35]. In both cases, fully saturated moist air enters at 65 °C and cold saline feed enters the coil at 25 °C. The temperature profiles are plotted against the normalized enthalpy, which is the change in enthalpy from the cold end over the total enthalpy change. With multistaging, the outlet temperature of the air is nearly 25°C lower and the outlet temperature of the saline stream is 10°C higher. Thus, the effectiveness of the device is substantially increased.

Figure 9.29 illustrates the increase in effectiveness of the device with multistaging. The experimental data presented here is for an air inlet temperature of 65 °C, inlet relative humidity of 100%, a water inlet temperature of 25 °C, and a water-to-air mass flow rate ratio of 2.45. It can be seen that the energy effectiveness of the device is increased from around 54for a single

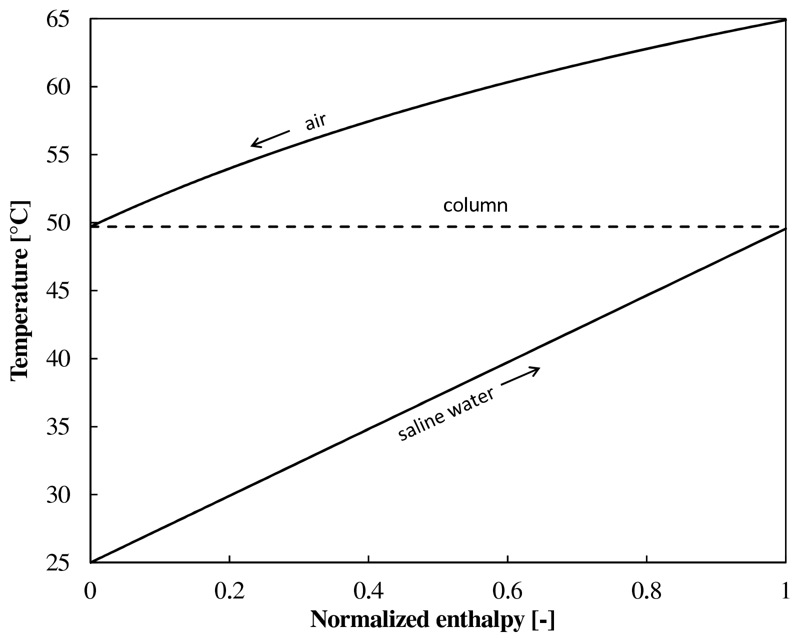

(a) Single-tray bubble column.

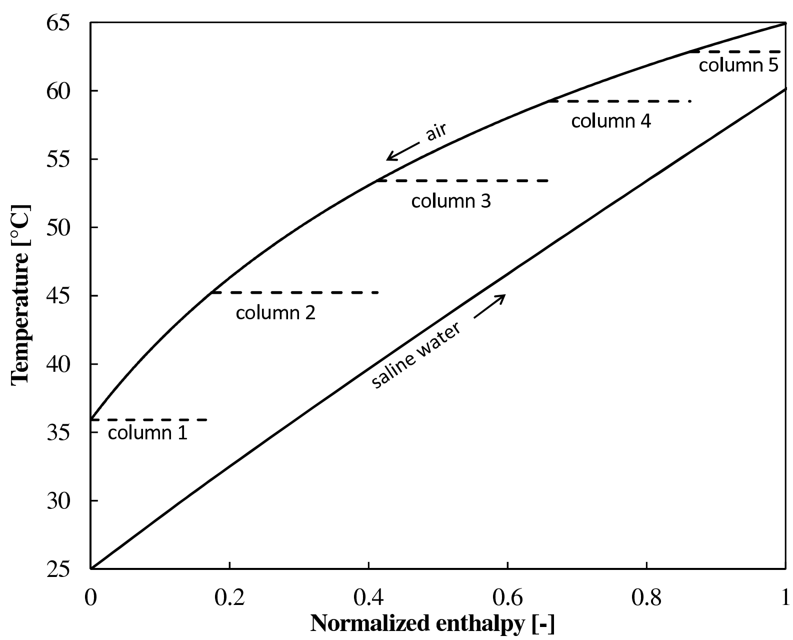

(b) Five-tray bubble column.

Figure 9.28: Comparison of the performance of a single-tray bubble column and a five-tray bubble column. Both dehumidifiers have the same size, and operate under the same conditions. In the multi-tray dehumidifier, the coil length is divided equally between the trays [35].

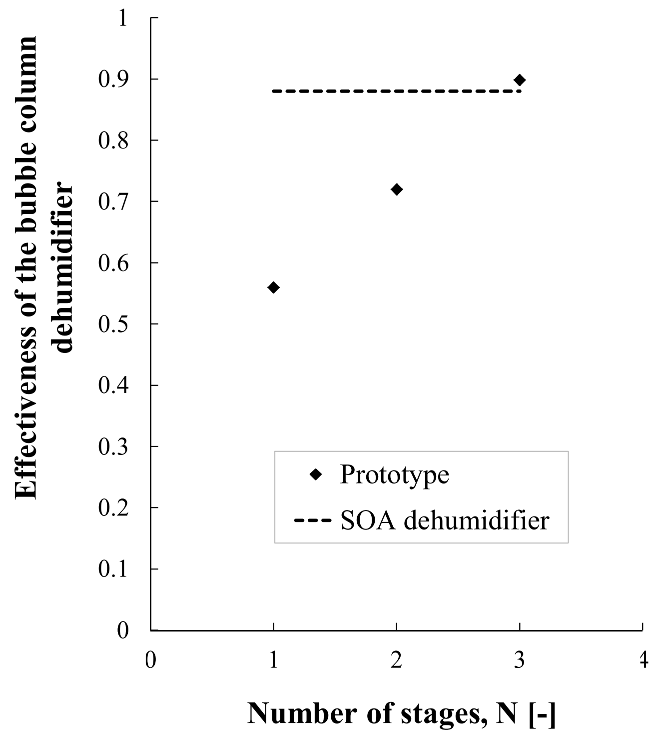

Figure 9.29: Effect of multistaging the bubble column on energy effectiveness of the device in comparison to a state-of-the-air (SOA) polypropylene plate-and-tube dehumidifier [3, 85, 91].

stage to about 90% for the three stage device. Further, owing to the higher superficial velocity (because of smaller column diameter), the heat fluxes were much higher (up to 25 kW/m^2) than for film-condensation dehumidifiers. Also, the total gas side pressure drop of this device was modest at 800 Pa.

The advantages of the multi-stage bubble column relative to conventional dehumidifiers include a nearly order-of-magnitude reduction of surface area and volume with associated cost savings [91]. An important design consideration is to maintain a very shallow liquid pool depth in each tray, so as to limit the gas-side pressure loss. These same concepts have been extended to the development of bubble column humidifiers [92, 93].

9.4.3 Coil-free bubble columns

Industrial applications of HDH often involve saline feeds with a high fouling propensity, such as water produced in oil and gas extraction. In these situations circulating the feed through a bubble column coil can be problematic, as coils have small, curved passages that are not easily cleaned. This challenge has motivated the development of coil-free bubble columns [94], in which fresh water and moist air have a counterflow configuration (Fig. 9.30a). In the case shown, initially cool water (232) travels progressively from the upper to the lower trays, being warmed as water vapor condenses into it in each successive tray. The flow of water from tray to tray is regulated by weirs (228, 250). Warm fresh water is removed at the bottom (242). Warm, moist air enters the sparger at the bottom (240), and cool, dry air is removed at the top (230). The design shown uses just two trays, but in practice more trays are possible. In addition, this design shows how air extracted from a humidifier might be injected into the dehumidifier (205).

A separate heat exchanger is used to complete the necessary energy recovery from the fresh water stream, preheating the saline feed (Fig. 9.30b). This arrangement has the important advantage of localizing any fouling of significance into the liquid-to-liquid heat exchanger, which can be more easily cleaned.

9.5 Effect of high salinity feed on HDH performance

The thermophysical properties of water are changed by the presence of dissolved salts, and this in turn can make the performance of HDH systems dependent upon the salinity of the feed. For feeds at oceanographic salinities or below, McGovern et al. [28] have shown that using pure water properties introduces a calculation error of no more than 4–5%. The salinities encountered in brine concentration, as for water produced during oil and gas extraction, may be significantly higher.

Sharqawy et al. [95] and Nayar et al. [96] have provided comprehensive reviews of the variation of seawater properties with temperature, pressure, and salinity up to at least 120,000 g/kg. Nayar et al. [97] have also provided the surface tension of seawater over a broad range of salinity and temperature. For produced water, and ground water more generally, the ionic composition of dissolved salts can be highly variable, so that the properties of different samples must be found individually. Thiel and coworkers have made comprehensive use of the Pitzer-Kim model to provide such properties for various produced waters, ranging up to saturation concentrations [40, 98, 99].

Of particular importance to HDH systems are the variation in specific heat capacity and water vapor pressure (or boiling point elevation) with salinity. Figure 9.31 shows the variation of specific heat capacity of seawater with salinity and temperature [12]. Figure 9.32 shows the variation of boiling point elevation with the molality of dissolved salts [40]. Boiling point elevation can critically influence the temperature pinch in the humidifier, and changes in the specific heat capacity will directly affect the mass flow rate ratios needed to obtain $\mathrm{HCR}_d = 1$. Related issues are known to occur in seawater cooling towers [100] and in other saline evaporators [101].

Thiel et al. [40] have directly evaluated the effect of varied salinity on the performance of HDH cycles, using NaCl(aq) as a proxy for saline water and taking concentrations from 0 to 6 molal (near saturation). Their approach follows the saturation curve methodology introduced by McGovern et al. [28]. The process for analyzing the HDH system using a saturation curve (enthalpy-temperature, Fig. 9.33) approach is as follows. The top and bottom moist air temperatures $T_{ma,T}$ and $T_{ma,B}$ are chosen, which specifies the process path of the moist air. The mass flow rate ratio in the dehumidifier is chosen such that the pinch point temperature differences (ΔT_{pp}) in the dehumidifier are equal at both ends. This defines the feed process path in the dehumidifier. The ΔT_{pp} in the humidifier is then chosen; with the mass flow rate

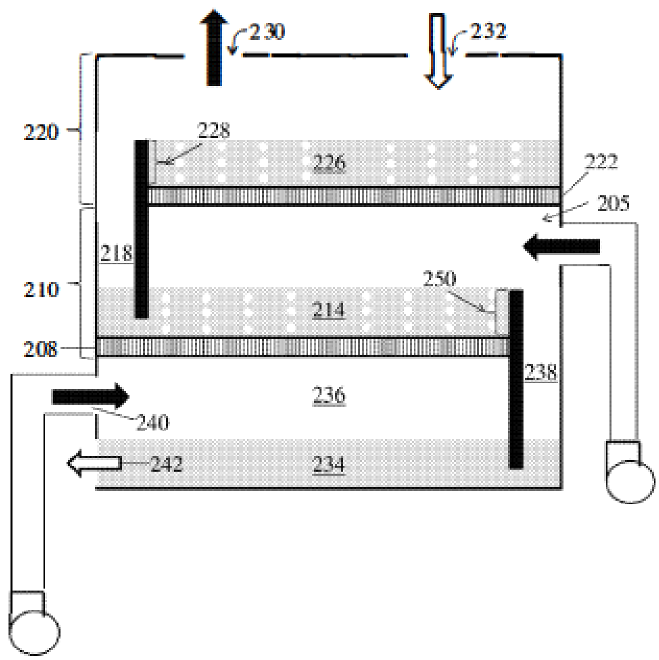

(a) Two tray coil-free bubble column.

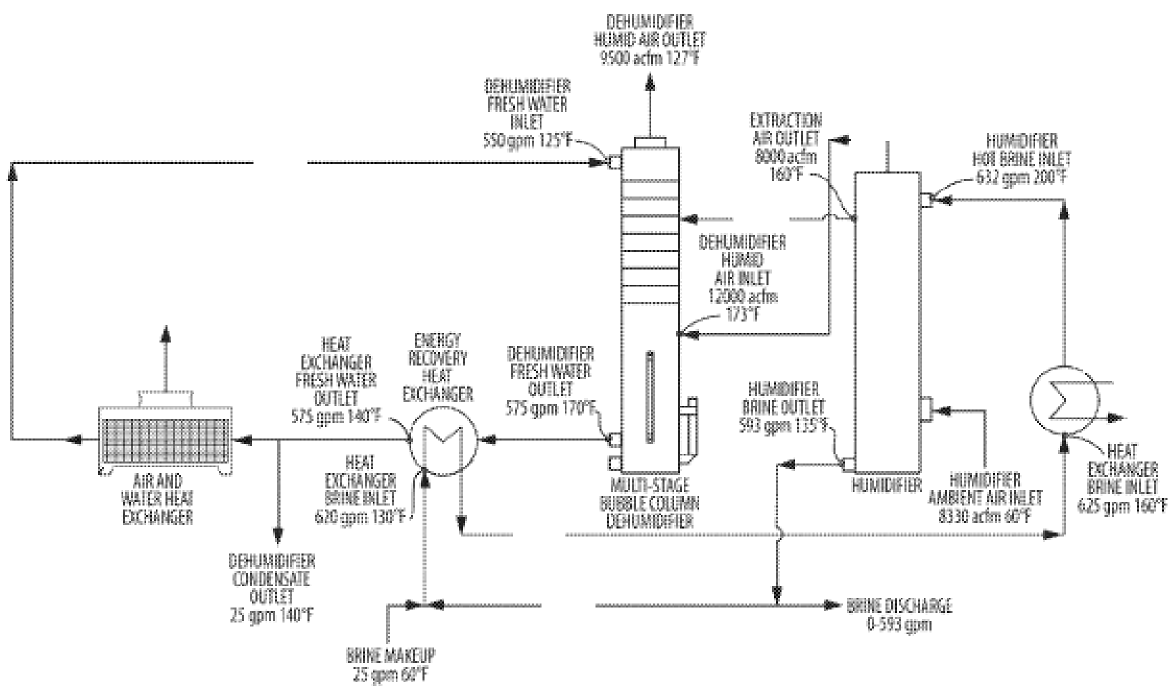

(b) HDH system with separate saline and fresh water loops.

Figure 9.30: Schematic diagrams of a coil-free dehumidifier implementation for an open-air, closed-water HDH system including air extraction/injection. Saline feed loop exchanges heat with fresh water loop through a separate heat exchanger [94].

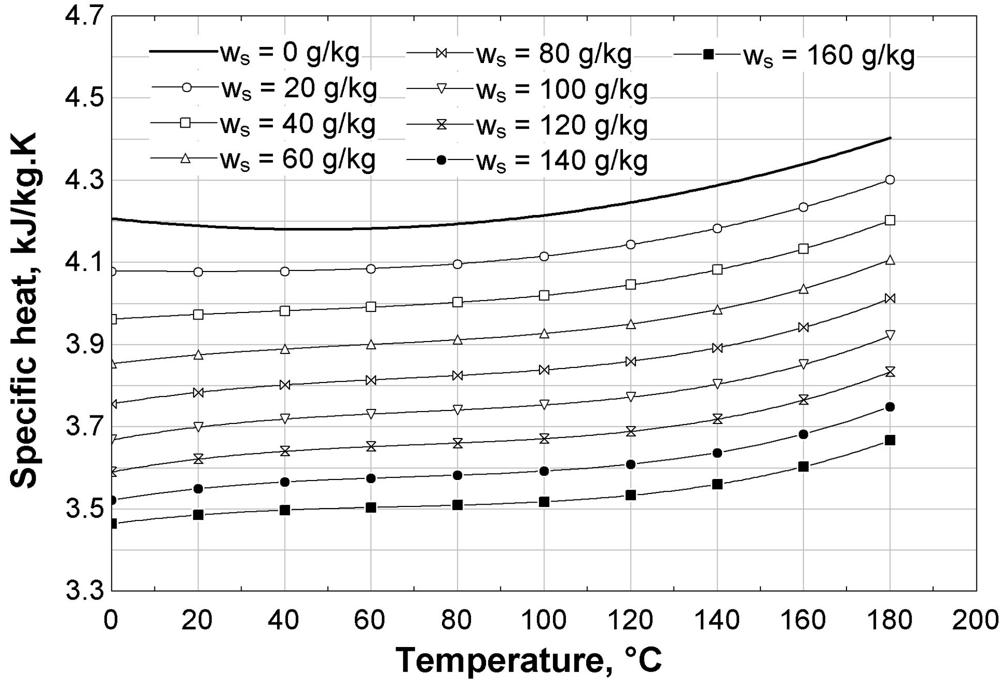

Figure 9.31: Variation of seawater specific heat capacity at constant pressure with salinity and temperature (w_s = mass fraction of salts) [12].

ratio, ΔT_{pp}, and top air temperature fixed, the brine process path in the humidifier is completely defined by energy conservation. See [40] for the analytical details. We note that this pinch-point analysis is another kind of on-design model.

The brine is recirculated in this analysis, with heat rejection after the outlet of the humidifier in order to return the brine to the dehumidifier inlet condition. Because the brine is recirculated and the per-cycle recovery is low, the brine salinity does not vary much between locations in the system. Thus, the saturation curve in the humidifier (H) is determined by the brine salinity and differs from the pure water curve in the dehumidifier (D). The effective boiling point elevation, δ_{eff}, for the saturation curves is shown in Fig. 9.33 and discussed in more detail in [40].

The GOR for the HDH system at high salinity versus ΔT_{pp} is shown in Fig. 9.34(a), benchmarked against the zero and single extraction cases at zero salinity from McGovern et al. [28]. In the high salinity, zero extraction case, GOR is reduced by about 17–27% relative to the zero salinity, zero extraction case. Owing to the effective boiling point elevation, the temperature to which the feed can be preheated is limited, resulting in a greater required heat input. In addition, because of the vapor pressure depression, the highest humidity ratio for air in contact with a saline stream at $T_{ma,T}$ is lower than for air in contact with a pure water stream at the same temperature. The recovery ratio (in a single pass) for a system operating between the same top and bottom air temperatures is thus reduced. The reduced water production and the limited preheat both reduce GOR.

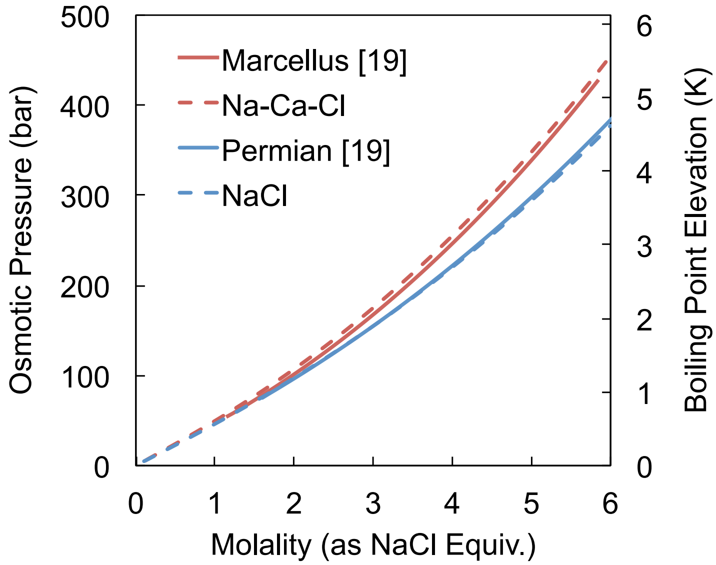

Figure 9.32: Boiling point elevation and osmotic pressure of typical produced water samples from [98] are well represented by aqueous NaCl. When Ca^{2+} concentrations are high, as for the Marcellus shale produced water, a mixture of Na-Ca-Cl in appropriate quantities is a better representation [40].

The second law efficiency of a desalination system compares the least work (exergy) of separation to the actually exergy input to the system, as discussed in detail in [12, 23, 40, 102, 103]. A fully reversible system has a second law efficiency of unity; any real system has lower efficiency. The least work increases with feed salinity, and the second law efficiency is generally higher for thermal systems when feed salinity rises [40]. Mistry et al. have examined the role of composition and salinity in changing the least work of separation [104,105]. Similarly, Ahdab et al. [106] have evaluated the dependence of least work on composition for a vast set of 28,000 ionically-complete USGS groundwater samples.

The second law efficiency for this HDH cycle is shown in Fig. 9.34(b), where the curves tend to increase with increasing feed salinity. When the brine salinity is high, the thermal energy consumption of HDH is essentially invariant with feed-salinity. As a result, because the least work is higher at higher feed salinities, the system operates closer to its reversible limit as feed salinity is increased.

Acknowledgements

This chapter draws heavily on published research done over a period of years with my graduate students and collaborators, including: Prof. Mohammed A. Antar, Dr. Karim M. Chehayeb, Dr. Prakash Narayan Govindan, Dr. Karan H. Mistry, Prof. Mostafa H. Sharqawy, Dr. Edward K. Summers, Dr. Gregory P. Thiel, Prof. Emily W. Tow, and Prof. Syed M. Zubair. Dr. Govindan also co-authored a previous version of this material.

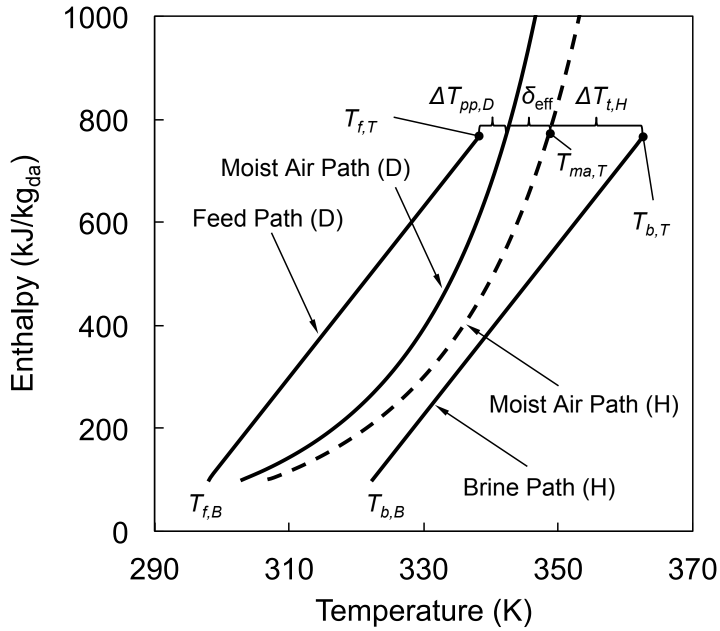

Figure 9.33: Process paths of feed, brine, and air streams in a zero extraction HDH system on an enthalpy-temperature diagram: the top and bottom air temperatures are 70°C and 25°C, respectively [40].

Nomenclature

Acronyms

AH	Air Heated
CAOW	Closed-Air, Open-Water cycle
GOR	Gained Output Ratio
HCR	Heat Capacity Rate Ratio
HDH	Humidification Dehumidification
HME	Heat and Mass Exchanger
PR	Performance Ratio
RR	Recovery Ratio
SEC	Specific Electricity Consumption
TTD	Terminal Temperature Difference
WH	Water Heated

Symbols

$\dot{H}$	total enthalpy flow rate (W)
h	specific enthalpy (J/kg)
h^*	specific enthalpy (J/kg dry air)
h_{fg}	spec. enthalpy of vaporization (J/kg)
m_r	water-to-air mass flow rate ratio (-)
$\dot{m}$	mass flow rate (kg/s)
N	number of extractions (-)
$\dot{Q}$	in heat transfer rate into heater (W)
$\dot{S}_{\text{gen}}$	entropy generation rate (W/K)
T	temperature (°C)
$\dot{W}_e$	electrical power (W)

Greek

δ_{eff}	effective boiling-point elevation (K)
Δ	difference or change
ε	energy based effectiveness (-)
Ψ	enthalpy pinch (kJ/kg dry air)
Ψ_{TD}	terminal enthalpy pinch (kJ/kg dry air)
ϕ	relative humidity (-)

Subscripts

a	humid air
b	brine
B	bottom
c	cold stream
d	humidifier value
deh	dehumidifier
da	dry air
f	feed

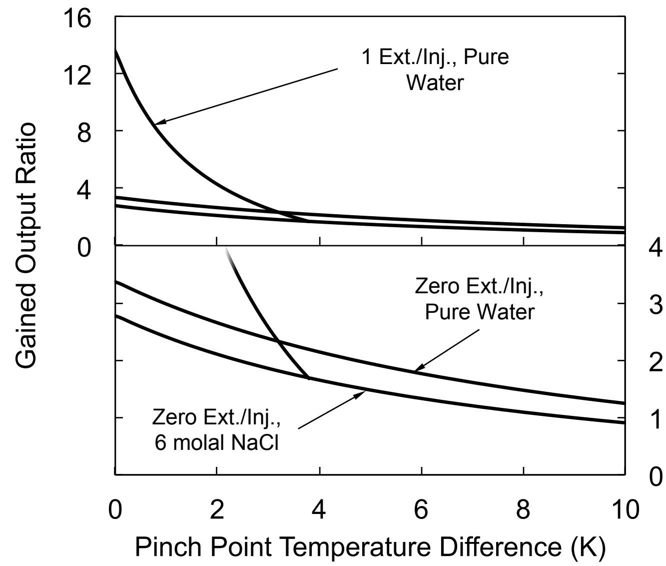

(a) $T_{ma,T} = 70°C$, $T_{f,B} = 25°C$

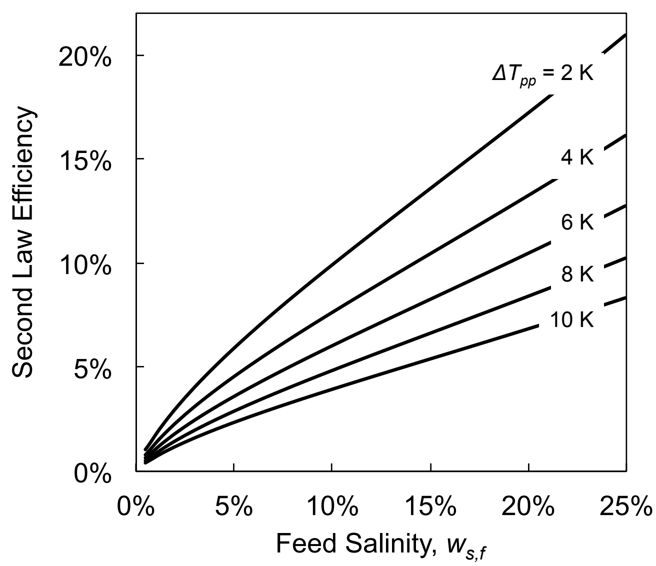

(b) $T_{ma,T} = 70°C$, $T_{f,B} = 25°C$

Figure 9.34: Energetic figures of merit for HDH over the salinity domain: (a) GOR, benchmarked against zero salinity data from [28], and (b) efficiency. Because HDH is inherently low recovery in a single pass, the brine recirculation configuration required for high recovery wastewater treatment means that the system always operates at the highest (brine) salinity, and has energy consumption that is insensitive to feed salinity [40].

h	hot stream or humidifier value
hum	humidifier
i	inlet value
ma	moist air
max	maximum
local	defined locally
o	lowest temperature
pinch	pinch point value
pp	pinch point
pw	pure water
s	steam
T	top
th	thermal
w	saline water

Thermodynamic states

a	Seawater entering the dehumidifier
b	Preheated seawater leaving the dehumidifier
c	Seawater entering the humidifier from the brine heater
d	Brine reject leaving the humidifier
e	Moist air entering the dehumidifier
ex	Moist air state at which mass extraction and injection is carried
out	in single extraction cases
f	Relatively dry air entering the humidifier

References

1) G.P. Narayan, M.H. Sharqawy, E.K. Summers, J.H. Lienhard V, S.M. Zubair, M.A. Antar, The potential of solar-driven humidification–dehumidification desalination for small-scale decentralized water production, *Renew. Sust. Energy Rev.* **14**, 1187–1201 (2010).
2) T. Pankratz (ed.), HDH tackles brine disposal challenge, *Water Desalination Report*, **50**, 2–3, May 2014.
3) G.P. Narayan, *Thermal Design of Humidification Dehumidification Systems for Affordable, Small-scale Desalination*. PhD thesis, Massachusetts Institute of Technology (2012).
4) A. Giwa, N. Akther, A. Al Housani, S. Haris, S.W. Hasan, Recent advances in humidification dehumidification (HDH) desalination processes: Improved designs and productivity, *Renew. Sust. Energy Rev.* **57**, 929–944 (2016).
5) B. Seifert, A. Kroiss, M. Spinnler, T. Sattelmayer, About the history of humidification-dehumidification desalination systems, *The International Desalination Association World Congress on Desalination and Water Reuse 2013*, Tianjin, China Paper No. IDAWC/TIAN13-375.
6) G. N. Tiwari, H. N. Singh, and R. Tripathi, Present status of solar distillation, *Solar Energy* **75(5)**, 367–373 (2003).
7) H. E. S. Fath, Solar distillation: a promising alternative for water provision with free energy, simple technology and a clean environment, *Desalination*, **116**, 45–56 (1998).
8) T. A. Lawand, *Systems for solar distillation*, Tech. Rep., Brace Research Institute, Report No. R115, Sep. (1975).
9) Hodges, C.N., Thompson, T.L., Groh, J.E., Seller, W.D., The Utilization of Solar Energy in a Multiple-Effect Desalination System, *J. Applied Meteorology* **3(5)**, 505–512 (1964).
10) T. Pankratz (ed.), Investor opens door to Chinese market, *Water Desalination Report* **52(33)**, 29 August 2016.
11) Y. Li, J. F. Klausner, and R. Mei, Performance characteristics of the diffusion driven desalination process, *Desalination* **196**, 188–196 (2006).
12) J.H. Lienhard V, K.H. Mistry, M.H. Sharqawy, and G.P. Thiel, Thermodynamics, Exergy, and Energy Efficiency in Desalination Systems, in *Desalination Sustainability: A Tech-*

nical, Socioeconomic, and Environmental Approach, Chpt. 4, H.A. Arafat, ed. Elsevier Publishing Co., 23 June 2017.

13) G. Al-Enezi, H. Ettouney, and N. Fawzi, Low temperature humidification dehumidification desalination process, *Energy Conversion Manag.* **47**, 470–484, 2006.
14) B. M. Hamieh, J. R. Beckman, and M. D. Ybarra, Brackish and seawater desalination using a 20 sq. ft. dewvaporation tower, *Desalination* **140**, 217–226, 2001.
15) H. B. Bacha, T. Damak, and M. Bouzguenda, Experimental validation of the distillation module of a desalination station using the SMCEC principle, *Renewable Energy* **28**, 2335–]2354, 2003.
16) H. Müller-Holst, Solar thermal desalination using the Multiple Effect Humidification (MEH) method in *Solar Desalination for the 21st Century*, ch. 15, pp. 215–225. NATO Security through Science Series, Springer, Dordrecht, 2007.
17) G. P. Narayan, M. H. Sharqawy, J. H. Lienhard V, and S. M. Zubair, Thermodynamic analysis of humidification dehumidification desalination cycles, *Desalination and Water Treatment* **16**, 339–353, 2010.
18) E. Chafik, A new type of seawater desalination plants using solar energy, *Desalination* **156**, 333–348, 2003.
19) I. Houcine, M. B. Amara, A. Guizani, and M. Mâalej, Pilot plant testing of a new solar desalination process by a multiple-effect-humidification technique, *Desalination* **196**, 105–124, 2006.
20) J. H. Huang, *Design of a mobile community level water treatment system based on humidification dehumidification desalination.* SB Thesis, Massachusetts Institute of Technology (2012).
21) K.H. Mistry, J.H. Lienhard V, S.M. Zubair, Effect of entropy generation on the performance of humidification–dehumidification desalination cycles, *Int. J. Therm. Sci.* **49** 1837–1847 (2010).
22) K. H. Mistry, A. Mitsos, and J. H. Lienhard V, Optimal operating conditions and configurations for humidification-dehumidification desalination cycles, *Int. J. Therm. Sci.* **50**, 779–789 (2011).
23) K.H. Mistry, R.K. McGovern, G.P. Thiel, E.K. Summers, S.M. Zubair, J.H. Lienhard V, Entropy generation analysis of desalination technologies, *Entropy* **13**, 1829–1864 (2011) .
24) G.P. Thiel, J.H. Lienhard V, Entropy generation in condensation in the presence of high concentrations of noncondensable gases, *Int. J. Heat Mass Transfer* **55**, 5133–5147 (2012).
25) G.P. Narayan, J.H. Lienhard V, S.M. Zubair, Entropy generation minimization of combined heat and mass transfer devices, *Int. J. Therm. Sci.* **49**, 2057–2066, (2010).
26) H. Müller-Holst, *Mehrfacheffekt-Feuchtluftdestillation bei Umgebungsdruck — Verfahrensoptimierung und Anwendungen*, PhD thesis, Technische Universität Berlin (2002).
27) M. Zamen, S.M. Soufari, M. Amidpour, Improvement of solar humidification-dehumidification desalination using multi-stage process, *Chem. Eng. Trans.* **25**, 1091–1096, (2011).
28) R.K. McGovern, G.P. Thiel, G.P. Narayan, S.M. Zubair, J.H. Lienhard V, Performance limits of zero and single extraction humidification-dehumidification desalination systems, *Appl. Energy* **102**, 1081–1090 (2013).
29) G.P. Narayan, K.M. Chehayeb, R.K. McGovern, G.P. Thiel, S.M. Zubair, J.H. Lienhard V, Thermodynamic balancing of the humidification dehumidification desalination system by mass extraction and injection, *Int. J. Heat Mass Transfer* **57(2)**, 756–770 (2013).

30) G.P. Narayan, M.G. St. John, S.M. Zubair, J.H. Lienhard V, Thermal design of the humidification dehumidification desalination system: an experimental investigation, *Int. J. Heat Mass Transfer* **58**, 740–748 (2013).
31) K.M. Chehayeb, G. Prakash Narayan, S.M. Zubair, J.H. Lienhard V, Use of multiple extractions and injections to thermodynamically balance the humidification dehumidification desalination system, *Int. J. Heat Mass Transfer* **68**, 422–434 (2014).
32) M. Poppe and H. Rögener, Berechnung von rückkühlwerken," VDI-Wärmeatlas, **111**, 1–15 (1991).
33) J. Kloppers and D. Kröger, A critical investigation into the heat and mass transfer analysis of counter ow wet-cooling towers," *Int. J. Heat Mass Transfer* **48**, 765–777 (2005).
34) J. C. Kloppers, *A critical evaluation and refinement of the performance prediction of wet-cooling towers*, PhD thesis, University of Stellenbosch (2003).
35) K.M. Chehayeb, F.K. Cheaib, and J.H. Lienhard V, A numerical solution algorithm for a heat and mass transfer model of a desalination systems based on packed-bed humidification and bubble column dehumidification, in *Proc. 15th Intl. Heat Transfer Conference, IHTC-15*, no. IHTC15-8995, Kyoto, Japan (2014).
36) K.M. Chehayeb, G.P. Narayan, S.M. Zubair, and J.H. Lienhard V, Thermodynamic balancing of a fixed-size two-stage humidification dehumidification desalination system, *Desalination* **369**, 125–139 (2015).
37) F. Alnaimat, J.F. Klausner, Solar diffusion driven desalination for decentralized water production, *Desalination* **289**, 35–44, (2012).
38) G. P. Narayan, K. H. Mistry, M. H. Sharqawy, S. M. Zubair, and J. H. Lienhard V, Energy effectiveness of simultaneous heat and mass exchange devices, *Frontiers in Heat and Mass Transfer* **1**, 1–13 (2010).
39) A. Bejan, *Entropy generation minimization: the method of thermodynamic optimization of finite size systems and finite time processes*. Boca Raton, FL: CRC Press (1996).
40) G.P. Thiel, E.W. Tow, L.D. Banchik, H.W. Chung, J.H. Lienhard V, Energy consumption in desalinating produced water from shale oil and gas extraction, *Desalination* **366**, 94–112 (2015).
41) S. Al-Hallaj, M. M. Farid, and A. R. Tamimi, Solar desalination with humidification-dehumidification cycle: performance of the unit, *Desalination* **120**, 273–280, 1998.
42) S. Soufari, M. Zamen, and M. Amidpour, "Performance optimization of the humidification-dehumidification desalination process using mathematical programming," *Desalination* **237**, 305–317, 2009.
43) M. M. Farid and A. W. Al-Hajaj, "Solar desalination with humidificationdehumidification cycle," *Desalination* **106**, 427–429, 1996.
44) N. K. Nawayseh, M. M. Farid, S. Al-Hajaj, and A. R. Tamimi, Solar desalination based on humidification process-I. evaluating the heat and mass transfer coefficients, *Energy Conversion Manage.* **40**, 1423–1449, 1999.
45) M. Ben Amara, I. Houcine, A. Guizani, and M. Mâalej, Experimental study of a multiple-effect humidification solar desalination technique, *Desalination* **170**, 209–221, 2004.
46) C. Yamali and I. Solmus, A solar desalination system using humidification– dehumidification process: experimental study and comparison with the theoretical results, *Desalination* **220**, 538–551, 2008.
47) E. Chafik, Design of plants for solar desalination using the multi-stage heating/ humidi-

fying technique, *Desalination* **168**, 55–71, 2004.

48) G.P. Narayan, R.K. McGovern, S.M. Zubair, and J.H. Lienhard V, High-temperature-steam-driven, varied-pressure, humidification-dehumidification system coupled with reverse osmosis for energy-efficient seawater desalination, *Energy*, **37(1)**, 482-493, (2012).
49) G.P. Narayan, R.K. McGovern, J.H. Lienhard V, and S.M. Zubair, Variable pressure humidification dehumidification desalination systems, *Proc. 8th ASME/JSME Thermal Engineering Joint Conf.*, Honolulu (2011).
50) F. Al-Sulaiman, G.P. Narayan, and J.H. Lienhard V, Exergy Analysis of a High-Temperature-Steam-Driven, Varied-pressure, Humidification-Dehumidification System Coupled with Reverse Osmosis, *Applied Energy* **103**, 552–561 (2013).
51) R.K. McGovern, G.P. Narayan, and J.H. Lienhard V, Analysis of Reversible Ejectors and Definition of Ejector Efficiency, *Int. J. Therm. Sci.* **54(4)**, 153–166 (2012).
52) R.K. McGovern, K.V. Bulusu, M.A. Antar, and J.H. Lienhard V, One-dimensional Model of an Optimal Ejector and Parametric Study of Ejector Efficiency, *25th Intl. Conf. on Efficiency, Cost, Optimization, Simulation (ECOS) and Environmental Impact of Energy Systems*, Perugia, Italy (2012).
53) Y.S. Perez Zuniga, *Design of an Axial Turbine and Thermodynamic Analysis and Testing of a K03 Turbocharger*, S.B. Thesis, Massachusetts Institute of Technology (2011).
54) G.P. Narayan, R.K. McGovern, J.H. Lienhard V, and S.M. Zubair, Helium as a Carrier Gas in Humidification Dehumidification Desalination Systems, *Proc. ASME 2011 Intl. Mech. Engr. Cong. & Exp.*, Denver (2011).
55) E.W. Tow and J. H. Lienhard V, Experiments and modeling of bubble column dehumidifier performance, *Int. J. Therm. Sci.* **80**, 65–75 (2014).
56) E.W. Tow, J.H. Lienhard V, Analytical modeling of a bubble column dehumidifier, *Proc. ASME 2013 Summer Heat Transfer Conf.*, Paper No. HT2013-17763, Minneapolis, MN (2013).
57) G.P. Thiel, R.K. McGovern, S.M. Zubair, and J.H. Lienhard V, Thermodynamic equipartition for increased second law efficiency, *Applied Energy* **118**, 292–299 (2014).
58) E.K. Summers, M.A. Antar, and J.H. Lienhard V, Design and optimization of an air heating solar collector with integrated phase change material energy storage for use in humidification-dehumidification desalination, *Solar Energy* **86(11)**, 3417–3429 (2012).
59) E.K. Summers, J.H. Lienhard V, and S.M. Zubair, Air-heating solar collectors for humidification-dehumidification desalination systems, *J. Solar Energy Engrg.* **113(1)**, 011016 (2011).
60) G.P. Thiel, J.A. Miller, S.M. Zubair, and J.H. Lienhard V, Effect of mass extractions and injections on the performance of a fixed-size humidification-dehumidification desalination system, *Desalination* **314**, 50–58 (2013).
61) J.A. Miller and J.H. Lienhard V, Impact of Extraction on a Humidification-Dehumidification Desalination System, *Desalination* **313**, 87–96, (2013).
62) A. P. Colburn and O. A. Hougen, Design of cooler condensers for mixtures of vapors with noncondensing gases, *Ind. Eng. Chem.* **26**, 1178–1182 (1934).
63) W. Nusselt, Die oberflachenkondensation des wasserdampfes, *Zeitschrift des Vereins-DeutscherIngenieure* **60**, 541–546, 1916.
64) E. M. Sparrow and E. R. G. Eckert, Effects of superheated vapor and noncondensable gases on laminar film condensation, *AIChE J.* **7**, 473–477, 1961.
65) E. M. Sparrow, W. J. Minkowycz, and M. Saddy, Forced convection condensation in the

presence of noncondensables and interfacial resistance, *Int. J. Heat Mass Transfer* **10**, 1829–1845, 1967.

66) W. J. Minkowycz and E. M. Sparrow, Condensation heat transfer in the presence of noncondensables: interfacial resistance, superheating, variable properties, and diffusion, *Int. J. Heat Mass Transfer* **9**, 1125–1144, 1966.

67) V. E. Denny, A. F. Mills, and V. J. Jusionis, Laminar film condensation from a steam-air mixture undergoing forced flow down a vertical surface, *J. Heat Transfer* **93**, 297–304, 1971.

68) V. E. Denny and V. J. Jusionis, Effects of noncondensable gas and forced flow on laminar film condensation, *Int. J. Heat Mass Transfer* **15**, 315–326, 1972.

69) C. Y. Wang and C. J. Tu, Effects of non-condensable gas on laminar film condensation in a vertical tube, *Int. J. Heat Mass Transfer* **31**, 2339–2345, 1988.

70) T. Kageyama, P. F. Peterson, and V. E. Schrock, Diffusion layer modeling for condensation in vertical tubes with noncondensable gases, *Nucl. Eng. Des.* **141**, 289–302, 1993.

71) H. A. Hasanein, Steam condensation in the presence of noncondensable gases under forced convection conditions. PhD thesis, Massachusetts Institute of Technology, 1994.

72) S. Z. Kuhn, Investigation of heat transfer from condensing steam-gas mixture and turbulent films flowing downward inside a vertical tubes. PhD thesis, University of California at Berkeley, 1995.

73) N. K. Maheshwari, P. K. Vijayan, and D. Saha, Effects of non-condensable gases on condensation heat transfer, in Proceedings of 4th RCM on the IAEA CRP on Natural Circulation Phenomena, 2007.

74) H. A. Hasanein, M. S. Kazimi, and M. W. Golay, Forced convection in-tube steam condensation in the presence of noncondensable gases, *Int. J. Heat Mass Transfer* **39**, 2625–2639, 1996.

75) M. Siddique, M. W. Golay, and M. S. Kazimi, Local heat transfer coefficients for forced convection condensation of steam in a vertical tube in the presence of air, Two-Phase Flow and Heat Transfer (3rd ed.), ASME, New York, 197, 386–402, 1992.

76) V. D. Rao, V. M. Krishna, K. V. Sharma, and P. M. Rao, Convective condensation of vapor in the presence of a non-condensable gas of high concentration in laminar flow in a vertical pipe, *Int. J. Heat Mass Transfer* **51**, 6090–6101, 2008.

77) B. M. Hamieh and J. R. Beckman, Seawater desalination using dewvaporation technique: experimental and enhancement work with economic analysis, *Desalination* **195**, 14–25, 2006.

78) M. A. Sievers and J. H. Lienhard V, "Design of flat-plate dehumidifiers for humidification dehumidification desalination systems," *Heat Transfer Engrg.* **34(7)**, 543–561, 2013.

79) M. A. Sievers and J. H. Lienhard V, "Design of Plate-Fin Tube Dehumidifiers for Humidification-Dehumidification Desalination Systems," *Heat Transfer Engnrg.* **36(3)**, 223–243 (2015).

80) A. V. Kulkarni and J. B. Joshi, Design and selection of sparger for bubble column reactor. part i: Performance of different spargers, *Chem. Eng. Res. Des.* **89**, 1972–1985, 2011.

81) J. B. Joshi and M. M. Sharma, A circulation cell model for bubble columns, *Chem. Eng. Res. Des.* **57a**, 244–251, 1979.

82) G. P. Narayan, M. H. Sharqawy, S. Lam, and J. H. Lienhard V, Bubble columns for condensation at high concentrations of non-condensable gas: heat transfer model and experiments, *AIChE J.* **59(5)**, 1780–1790, (2013).

83) E. W. Tow and J. H. Lienhard V, "Heat flux and effectiveness in bubble column dehumidifiers for HDH desalination," Proc. IDA World Congress on Desalination and Water Reuse, Tianjin, China, 2013.
84) E.W. Tow and J.H. Lienhard V, Heat transfer to a horizontal cylinder in a shallow bubble column, *Intl. J. Heat Mass Transfer*, **79**:353–361 (2014).
85) G.P. Narayan and J.H. Lienhard V, Thermal Design of Humidification Dehumidification Systems for Affordable Small-scale Desalination, *IDA Journal*, **4(3)**:24–34 (2012).
86) G.P. Narayan, G.P. Thiel, R.K. McGovern, J.H. Lienhard V, and M.H. Sharqawy, Multi-Stage Bubble Column Dehumidifier, US Patent #8525447 (2013).
87) G.P. Narayan, G.P. Thiel, R.K. McGovern, J.H. Lienhard V, and M.H. Sharqawy, Humidification-Dehumidification System Including Bubble Column Vapor Mixture Condenser, US Patent #8778065 (2014).
88) G.P. Narayan, G.P. Thiel, R.K. McGovern, J.H. Lienhard V, and M.H. Sharqawy, Bubble Column Vapor Mixture Condenser, US Patent #9072984 (2015).
89) Humidification-Dehumidification System with a Bubble-Column Vapor Mixture Condenser and Intermediate Gas Extraction, G.P. Narayan, G.P. Thiel, R.K. McGovern, J.H. Lienhard V, and M.H. Sharqawy, US Patent #9320984 (2016).
90) G.P. Narayan, G.P. Thiel, R.K. McGovern, J.H. Lienhard V, and M.H. Sharqawy, Multistage Bubble-Column Vapor Mixture Condenser, US Patent #9403104 (2016).
91) S. Lam, *Development of a multi-stage bubble column dehumidifier for application in a humidification dehumidification desalination system.* SB Thesis, Massachusetts Institute of Technology (2012).
92) G.P. Narayan, M.H. Sharqawy, J.H. Lienhard V, S. Lam, and M. St. John, Multistage bubble column humidifier, US Patent #9120033 (2015).
93) G.P. Narayan, M.H. Sharqawy, J.H. Lienhard V, S.Lam, and M. St. John, Multistage bubble column humidifier, US Patent #9790102 (2017).
94) G.P. Narayan, S.Lam, and M. St. John, Systems including a condensing apparatus such as a bubble column condenser, US Patent #9700811 (2017).
95) M.H. Sharqawy, J.H. Lienhard V, and S.M. Zubair, The thermophysical properties of seawater: A review of existing correlations and data, *Desalination and Water Treatment*, **16**:354–380 (2010).
96) K.G. Nayar, M.H. Sharqawy, L.D. Banchik, and J.H. Lienhard V, "Thermophysical properties of seawater: A review and new correlations that include pressure dependence," *Desalination*, **390**:1-24, 15 July 2016
97) K.G. Nayar, D. Panchanathan, G.H. McKinley, and J.H. Lienhard V, "Surface tension of seawater," *J. Phys. Chem. Ref. Data*, **43(4)**:43103, Nov. 2014.
98) G.P. Thiel and J.H. Lienhard V, "Treating produced water from hydraulic fracturing: composition effects on scale formation and desalination system selection," *Desalination*, **346**:54-69, May 2014.
99) G.P. Thiel, S.M. Zubair, and J.H. Lienhard V, "An analysis of likely scalants in the treatment of produced water from Nova Scotia," *Heat Transfer Engineering*, **36(7-8)**:652-662, 2015.
100) M.H. Sharqawy, J.H. Lienhard V, and S.M. Zubair, On thermal performance of seawater cooling towers, *J. Engineering for Gas Turbines and Power*, **133(4)**:043001 (2011).
101) G.P. Thiel and J.H. Lienhard V, "An effectiveness-NTU relationship for evaporators with non-negligible boiling point elevation increases," *J. Heat Transfer*, **138(12)**:12180,

Dec. 2016.

102) K. Mistry and J.H. Lienhard V, “Generalized least energy of separation for desalination and other chemical separation processes,” *Entropy*, **15(6)**:2046–2080, May 2013.

103) E.W. Tow, R.K. McGovern, and J.H. Lienhard V, “Raising forward osmosis brine concentration efficiency through flow rate optimization,” *Desalination*, **366**:71–79, 15 June 2015.

104) K. Mistry, H.A. Hunter, and J.H. Lienhard V, “Effect of composition and nonideal solution behavior on desalination calculations for mixed electrolyte solutions with comparison to seawater,” *Desalination*, **318**:34–47, June 2013.

105) K.H. Mistry and J.H. Lienhard V, “Effect of Nonideal Solution Behavior on Desalination of a Sodium Chloride (NaCl) Solution and Comparison to Seawater,” *J. Energy Res. Tech.*, **135(4)**:042003, Dec. 2013.

106) Y. Ahdab, G.P. Thiel, J.K. Böhlke, J. Stanton, and J.H. Lienhard V, “Minimum energy requirements for desalination of brackish groundwater in the United States with comparison to international datasets,” *Water Research*, **141**, 387–404, 15 Sept. 2018.